Regulatory T cell-derived enkephalin imparts pregnancy-induced analgesia

Élora Midavaine[1], Beatriz C. Moraes[1], Jorge Benitez[1], Sian R. Rodriguez[1], Joao M. Braz[1], Nathan P. Kochhar[1], Walter L. Eckalbar[1], Ana I. Domingos[2], John E. Pintar[3], Allan I. Basbaum[1*], Sakeen W. Kashem[4,5*]

Affiliations:
[1]Department of Anatomy, University of California San Francisco, San Francisco, California, USA.
[2]Department of Physiology, Anatomy and Genetics, University of Oxford, Oxford, UK.
[3]Department of Neuroscience and Cell Biology, Rutgers Robert Wood Johnson Medical School, Piscataway, NJ, USA.
[4]Department of Dermatology, University of California San Francisco, San Francisco, CA, USA.
[5]Dermatology, Veterans Affairs Medical Center, San Francisco, California, USA.
*These authors contributed equally

Correspondence:
Allan I. Basbaum,
Chair and Professor, Department of Anatomy
University of California San Francisco
1550 Rock Hall, Room 345A, San Francisco, California, USA 94158
Email: allan.basbaum@ucsf.edu

Lead correspondence:
Sakeen W. Kashem
Assistant Professor, Dermatology
University of California San Francisco
1701 Divisadero, 3rd Floor, San Francisco, CA 94115
Email: sakeen.kashem@ucsf.edu

Keywords:
Pain, regulatory T cells, neuroimmunology, sex dimorphism, pregnancy, opioid, sensory neurons, enkephalin, meninges

Word count:
5026 (Main)
1676 (Main figure legend)

Summary
T cells have emerged as sex-dependent orchestrators of pain chronification but the sexually dimorphic mechanisms by which T cells control pain sensitivity is not resolved. Here, we demonstrate an influence of regulatory T cells (Tregs) on pain processing that is distinct from their canonical functions of immune regulation and tissue repair. Specifically, meningeal Tregs (mTregs) express the endogenous opioid, enkephalin, and mTreg-derived enkephalin exerts an antinociceptive action through a presynaptic opioid receptor signaling mechanism that is dispensable for immunosuppression. mTregs are both necessary and sufficient for suppressing mechanical pain sensitivity in female but not male mice. Notably, the mTreg modulation of pain thresholds depends on sex-hormones and expansion of enkephalinergic mTregs during gestation imparts a remarkable pregnancy-induced analgesia in a pre-existing, chronic, unremitting neuropathic pain model. These results uncover a fundamental sex-specific, pregnancy-pronounced, and immunologically-derived endogenous opioid circuit for nociceptive regulation with critical implications for pain biology and maternal health.

Graphical abstract

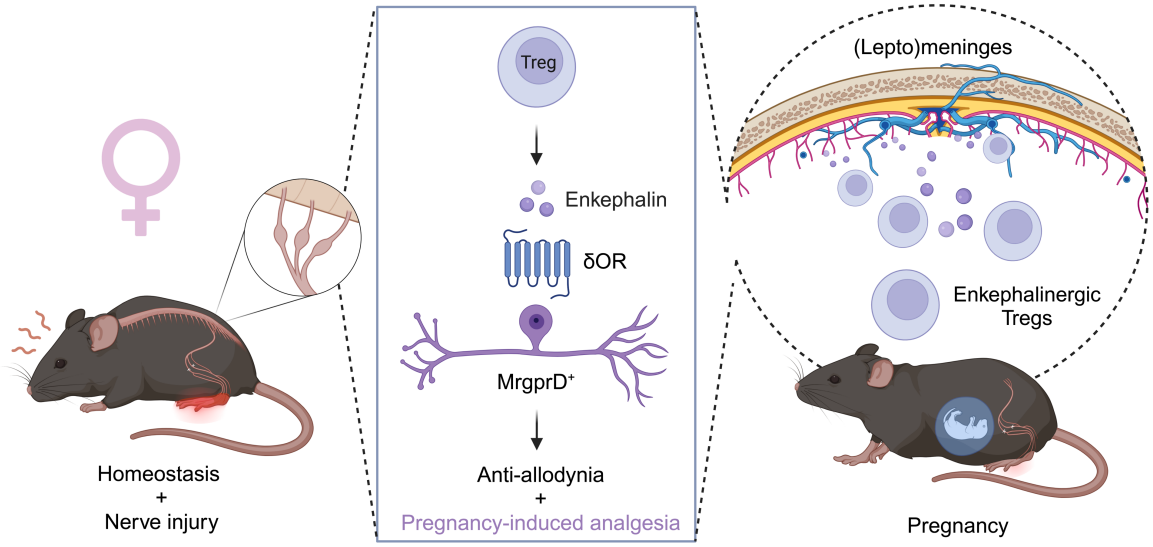

Highlights

1. Meningeal Treg expansion during gestation orchestrates pregnancy-induced analgesia
2. Gating of allodynia by meningeal Tregs is sex hormone-dependent
3. Treg-derived enkephalin modulates mechanical pain sensitivity, not inflammation
4. Delta opioid receptor on MrgprD^{+} sensory neuron mediates pain processing by mTregs

Introduction

Pain prevalence is significantly higher in women across multiple pain conditions including nerve injury-induced neuropathic pain, musculoskeletal pain, fibromyalgia and migraine[1]. Gender disparities in pain are further evidenced by notable changes in chronic pain severity during hormonal gender affirming care[2]. Moreover, chronic pain conditions, including migraine, can significantly improve over the course of pregnancy, in a phenomenon known as pregnancy-induced analgesia (PIA)[3,4]. Pregnancy-induced analgesia refers to a decrease in acute and pre-existing chronic pain during gestation[5–7]. Although the existence of PIA is acknowledged, its underlying mechanisms are unclear. Here, we identified a previously unknown immunological mechanism that underlies sex differences in both acute and chronic pain regulation. Finally, we demonstrate that this female-selective mechanism of pain modulation is co-opted during gestation, thus establishing pregnancy-induced analgesia.

Regulatory T cells (Tregs) are a subset of $CD4^+$ T cells characterized by their immunosuppressive function and the expression of the X-linked master regulatory transcriptional factor *Foxp3*. In addition to their critical function in limiting inflammation, Tregs are also major contributors to wound healing, they regulate stem cell turnover, maintain metabolic homeostasis, facilitate placental implantation and promote maternal-fetal tolerance[8–16]. In the context of nervous system injury, Tregs mitigate pro-inflammatory cytokine interferon-ɣ (IFN-ɣ)-driven mechanical pain hypersensitivity, suppress microglia-driven nociceptive processing and can reduce astrogliosis. Additionally, they contribute to improving remyelination, thereby promoting tissue repair[17–20]. However, whether and how Tregs can directly alter neuronal activity is still unknown.

Here, we demonstrate that meningeal regulatory T cells (mTregs) are essential contributors to baseline mechanical sensitivity, and to the inhibition of mechanical pain hypersensitivity (allodynia) after nerve injury, but only in female mice. Using a well-established spared-nerve injury (SNI) model of neuropathic pain, we further show that expanding mTregs can reduce nociceptive processing independently of Treg tissue repair programs. We find that mTregs produce the endogenous opioid met-enkephalin, with female mice exhibiting increased numbers of enkephalinergic mTregs. mTreg-derived enkephalin is required for the suppression of mechanical pain hypersensitivity, but not inflammation. This distinction reveals a novel Treg function that differs from their well-established roles in immunological restraint and tissue repair.

The involvement of distinct opioid receptors in the peripheral (PNS) and central nervous systems (CNS) in the regulation of different pain modalities is well documented. Delta (δOR) and mu (μOR) opioid receptors are differentially expressed among neuronal subsets and regulate mechanical or thermal pain processing, respectively[21–23]. Enkephalin can bind to both δOR and μOR, but preferentially engages the δOR. Here we demonstrate that the anti-allodynic effects derived from mTregs are mediated by the δOR that is expressed on the *Mas*-related G protein-coupled receptor member D (MrgprD) subset of unmyelinated primary sensory neurons.

Given the marked sex-difference observed in our findings of Treg-mediated suppression of nociceptive processing, we also investigated the determinants of this sex selectivity. We found that gonadal hormones, not sex chromosomes, influence the Treg suppression of nociceptive thresholds. Additionally, we demonstrate that mTregs significantly expand during pregnancy and release enkephalin, which via an action on δOR-expressing MrgprD^{+} sensory neurons to suppress chronic neuropathic pain. Thus, we present a novel pregnancy-protective mechanism of Tregs through their suppression of pre-existing maternal chronic pain.

Results

Sex-specific suppression of nociceptive thresholds by meningeal Tregs

As the immune system has emerged as a central determinant driving sex differences in pain sensitivity, we sought to investigate its contribution to nociceptive processing[24]. Tregs are a fundamental cell type essential for maintaining and restoring tissue homeostasis. Here we initially focused on identifying Treg localization and function within nervous system tissues. Using confocal microscopy and flow cytometry on whole meningeal sheets, dorsal root ganglia (DRG), sciatic nerves, spinal cords (SC) and brain, we localized Tregs to the meninges of the CNS, and to the leptomeninges of the DRG **(Figure 1A-C)**. To enhance the sensitivity of Treg detection within these organs, we utilized the bright reporter signals from the double reporter *Foxp3*$^{\text{eGFP-Cre-ERT2}}$*;Rosa26*$^{LSL\text{-}tdTomato}$ mice. Notably, and consistent with previous reports we observed a more pronounced localization of Tregs in the lumbar and caudal segments of the spinal cord meninges **(Figure 1A)** [25]. In the DRG, as for most leukocytes other than resident macrophages, Tregs predominated in the leptomeninges, proximal to the dorsal roots entry zone, with sparse presence within the DRG parenchyma **(Figure 1B)**[26]. By intravenous administration of a fluorescently-labeled CD45 antibody and using flow cytometry, we distinguished intravascular Tregs from tissue Tregs **(Figure S1A)**[27]. We quantified the numbers of non-vascular, tissue Tregs in various organs within the nervous and lymphoid systems. We will further refer to the SC meningeal and DRG leptomeningeal Tregs as mTregs **(Figure 1C)**. We observed minimal localization of Tregs in peripheral nerves and did not detect any Tregs within the parenchyma of the CNS in young, uninjured mice. We observed nearly equivalent numbers of tissue Tregs between male and female mice across tissue **(Figure 1D)**[18].

To assess the feasibility of site-specific depletion of mTregs, we performed intrathecal (IT) injections of pegylated diphtheria toxin (pegDT) in *Foxp3*-DTR mice[28]. Although an IT injection of Evan's blue rapidly spreads through the SC meninges and DRG, into the brain and to the draining cervical and lumbar lymph nodes, pegylated fluorescently labeled molecules (pegDyLight 650) remain restricted to the SC meninges and to the DRG **(Figure S2A-B)**. Consistently, a single 20 ng dose of pegDT IT selectively depleted >90% of SC and DRG mTregs in both male and female mice, but spared Tregs located in the brain meninges, draining lymph nodes, spleen, and peripheral nerves **(Figure 1E-F)**. Importantly, *Foxp3*-DTR mice subjected to repeated IT administrations of pegDT do not exhibit the significant weight loss, splenomegaly and mortality that typically develops following systemic autoimmunity in *Foxp3*-DTR mice induced by repeated intraperitoneal (IP) injections of diphtheria toxin (DT) **(Figure S2C-F)**. Clearly, the pegDT IT system offers a novel method for selective depletion of mTregs while avoiding systemic inflammation.

We next evaluated behavioral outcomes in mice following mTreg depletion. A single dose of pegDT IT induced a profound and prolonged decrease in mechanical thresholds in naïve female but not male *Foxp3*-DTR mice **(Figure 1G-H)**. Importantly, mechanical thresholds in wildtype (WT) C57BL/6 mice treated with pegDT IT or *Foxp3*-DTR mice treated with vehicle IT did not differ, ruling out pegDT or IT injections as the cause of the sex-specific allodynia **(Figure S3A)**. In addition to evaluating mechanical hypersensitivity,

which is conveyed by mechanosensitive unmyelinated and myelinated primary afferent nerve fibers, we also assessed mice for noxious heat sensitivity mediated by Trpv1^{+} nociceptors, cold sensitivity that is mediated by Trpm8^{+} nociceptors, pin prick sensitivity mediated by Aδ afferents and brush responses mediated by Aβ fibers. Although depletion of mTregs selectively induced mechanical allodynia in females, it did not impact any other sensory modality. Motor function tests using the rotarod also did not differ in either sex **(Figure 1I and Figure S3A-H)**. We conclude that mTregs selectively suppress mechanical thresholds in a sex-dependent manner, effectively preventing mechanical allodynia in a previously uninjured state.

Expansion of mTregs alleviates injury-induced mechanical allodynia independently of tissue repair

In addition to exploring mTreg role in mechanical sensitivity in uninjured mice, we investigated whether mTreg can suppress allodynia following nerve injury. Using a well-established spared nerve injury (SNI) model of neuropathic pain, we transected and ligated the common peroneal and tibial nerve branches of the sciatic nerve, sparing the sural nerve. This model induces chronic, unremitting, and permanent mechanical hypersensitivity with a non-healing neuroma formation four weeks after the injury **(Figure 2A-B)**[29,30]**.** As mice with SNI exhibit mechanical thresholds at the limit of detection with commercially available von Frey filaments, we conducted single fiber testing using the lowest available 0.008 g von Frey filament. Again, mTreg depletion increased allodynia following SNI in females, but not in males **(Figure 2C-D)**.

We next asked whether expanding mTregs could alleviate the mechanical allodynia independently of tissue repair. Tregs express the high affinity interleukin-2 receptor, IL-2Rα, and low-doses of IL-2 can effectively expand Tregs in mice, a therapeutic approach that has been used to treat autoimmune diseases in humans[31]. IT injections of low-dose IL-2 successfully expanded mTregs in both male and female mice **(Figure 2F)**. However, although mTreg expansion promoted significant anti-allodynia in SNI female mice, it did not exhibit a similar effect in males **(Figure 2G-H)**. It is noteworthy that acute IT injection of IL-2, in uninjured mice, did not increase nociceptive thresholds, suggesting that an IL-2 or Treg-based therapy could selectively improve neuropathic pain without affecting basal nociceptive processing **(Figure S4A-B)**. IL-2 injections and mTreg expansion in mice with SNI likewise did not alter noxious cold or heat sensitivity, again highlighting the specificity of the sensory modality modulation by mTreg in the context of neuropathic pain **(S4C-E)**.

Gonadal hormones, not sex chromosomes determine sex-selective, anti-nociceptive function of mTregs

Foxp3 is an X-linked gene, some of which escape X-inactivation. Moreover, random X-inactivation has been suggested to be potentially altered during inflammatory state in females[32–34]. To test whether sex chromosomes dosage contributes to our observed phenotype, we used the Four Core Genotypes (FCG) mouse model in which gonadal sex in mice is independent of sex chromosomes[35,36]. FCG mice harbor a deficiency in the sex determining region Y protein (*Sry*) on the Y chromosome and instead feature an autosomal transgenic insertion of *Sry.* This genetic configuration enables the

discrimination of sex chromosome dose influence from the contribution of gonadal hormones **(Figure 2I)**. Both XX and XY chromosome gonadal female mice displayed mTreg-mediated alleviation of mechanical allodynia after SNI; XX- and XY- gonadal male mice did not **(Figure 2J-L)**. Similarly, after mTreg depletion in *Foxp3*-DTR mice crossed to the FCG system, we found that female specific gonadal hormones, but not sex chromosome, mediate the mTreg suppression of nociceptive thresholds in the absence of injury **(Figure 2M-N)**. Based on our findings in both uninjured and chronic injury states, we conclude that there is a profound and consistent sex hormone-dependent contribution of mTregs to the modulation mechanical pain sensitivity.

Regulatory T cells express the endogenous opioid peptide enkephalin

To investigate the molecular mechanisms though which Tregs suppress nociceptive thresholds, we first interrogated public genomic resources. We hypothesized that meningeal tissue Tregs could exhibit an activated lymphoid Treg phenotype rather than a resting Treg phenotype. Tregs have increased expression of the *Penk* gene, which encodes for *Proenkephalin*, a peptide precursor of both Met- and Leu-enkephalin, in various tissues including the nervous system, in both mice and humans[19,37–39]. Here we re-analyzed raw public RNA-seq data of activated Tregs, resting Tregs, as well as activated and resting $CD4^+$ $Foxp3^-$ conventional T cells (Tconv)[40]. Strikingly, in activated versus resting Tregs, we observed a significant upregulation of *Penk* expression **(Figure 3A)**. We also investigated other opioid ligand and receptor genes but only recorded a very sparse expression of other opioid-related genes among the $CD4^+$ T cell subsets **(Figure 3B)**. Based on our prior experience defining mechanical sensitivity through enkephalin-δOR signaling[21], we therefore focused on Treg expression of *Penk.* By ATAC-seq analysis, we observed open chromatin regions of the *Penk* locus in activated Tregs, but not in other $CD4^+$ T cell subsets. This open chromatin was similar to the open chromatin, promoter and enhancer regions of the developing forebrain, an established enkephalin-producing area of the murine CNS **(Figure 3C)**[41]. By analyzing the raw dataset from the Immunological Genome Project[42], we also explored *Penk* expression within cell populations of the immune system. We observed a strikingly greater *Penk* expression in Tregs, compared to other immune cells (**Figure 3D)**. Furthermore, *Penk* expression in Tregs increase significantly following stimulation with IL-2, compared to other common gamma chain cytokines (**Figure 3E).**

To establish whether Tregs indeed produce the endogenous opioid peptide enkephalin, we screened commercially available anti-Met-enkephalin antibodies. Met-enkephalin was chosen over leu-enkephalin as the latter can be cleaved from both proenkephalin and prodynorphin peptides[43]. These antibodies were validated using *Penk*$^{-/-}$ mice as negative controls. Figure 3F shows that mTregs produce met-enkephalin, but meningeal $CD4^+$ T cells and lymphoid Tregs produce very low levels even after cytokine stimulation (**Figure 3F)**. We validated this finding by generating *Penk*^{Cre}*;Rosa26*^{tdTomato} mice, which fate-labeled enkephalinergic cells. Consistent with our antibody finding, we observed very similar number of enkephalinergic lineage (tdTomato positive) mTregs in naïve mice. Very few lymphoid or intravascular Tregs were tdTomato labeled **(Figure 3G)**. Most interestingly, female mice exhibited significantly greater numbers of enkephalin-positive

Tregs in the meninges, but not in the lymphoid organs. This distinction suggests that Treg fate and function variation across the sexes may be organ system specific **(Figure 3H)**.

mTreg-derived enkephalin is required for suppressing nociceptive processing

Using *Penk*^{Cre}*;Rosa26*^{tdTomato} mice, we next investigated enkephalin lineage positive cells in the meninges and the DRG. Interestingly, we observed a significant increase in the representation of mTregs in the tdTomato-positive enkephalin subpopulation compared to tdTomato-negative cells **(Figure 4A-B)**. In order to manipulate the enkephalin-producing immune cells, we generated bone marrow chimeric mice by transplanting *Penk*^{Cre}*;Rosa26*^{DTR} bone marrow into irradiated CD45.2 congenically marked WT mice **(Figure 4C)**. This strategy enables a selective DT-induced depletion of hematopoietic enkephalinergic cells, that spares depletion of non-hematopoietic enkephalinergic cells of the nervous system and the stroma. Importantly, CD4^{+} T cells of the meninges are predominantly bone marrow-derived and exhibit a tissue circulatory characteristic rather than acquiring tissue residency[44]. Consistently, we found that mTregs are indeed bone marrow-derived, similar to lymphoid Tregs, and differ from spinal microglia and skin Langerhans cells, which are host-derived **(Figure S5A-C)**. pegDT IT administrations in *Penk*DTR$^{\Delta heme}$ chimeric mice decreased the number of mTregs and led to profound mechanical hypersensitivity in female, but not male mice, in both uninjured and nerve injured states **(Figure 4D-G)**. We conclude that blood-derived meningeal enkephalinergic cells gate mechanical hypersensitivity in females.

Having established a female-specific contribution of the bone marrow-derived enkephalin system, we next used female mice to dissect the mechanism of pain regulation by mTregs. To establish whether bone marrow-derived enkephalin is required for the regulation of nociceptive thresholds, we generated bone marrow chimeras in which *Penk* deficient bone marrow is transplanted into irradiated hosts, thus generating *Penk*$^{\Delta heme}$ mice. As predicted, these *Penk*$^{\Delta heme}$ mice display decreased nociceptive thresholds during uninjured state, compared to vehicle-injected *Penk*$^{\Delta heme}$ mice, which supports our conclusion that hematopoietic cell-derived enkephalin controls basal mechanical sensitivity but only in females **(Figure 4H)**.

We recognize that recombination-based selective ablation of enkephalin on Tregs, using *Foxp3*^{Cre} or *Foxp3*$^{Cre\text{-}ERT2}$ has multiple limitations and caveats. These include systemic targeting of Tregs, including enkephalinergic Tregs in the skin, potential compensatory *Penk* regulation upon constitutive ablation, potential side effects of tamoxifen, potential stochastic deletion of *Penk* outside of Tregs in homozygote Cre/Cre-ERT2 mice, and the impact of random X-inactivation on heterozygous mice[37]. In light of these concerns, we also generated mixed bone marrow chimeras using 1:1 ratio of *Foxp3*-DTR and *Penk*$^{-/-}$ bone marrow and implanted these chimeras in irradiated WT mice. Intrathecal injection of pegDT into these mice results in ablation of *FoxP3*-DTR Tregs; the remaining Tregs are left deficient for *Penk* (*Penk*$^{\Delta mTreg}$ mice) while preserving other immune cell types. Importantly, this approach circumnavigated potential depletion of any previously unrecognized non-hematopoietic cells that express *Foxp3*. At baseline, uninjected mixed chimeric mice had similar mechanical thresholds as *WT*$^{\Delta heme}$ control chimeras. As predicted, pegDT IT injection led to mechanical hypersensitivity in uninjured *Penk*$^{\Delta mTreg}$

but not *WT*$^{\Delta heme}$ control mice and exacerbated nerve injury-induced hypersensitivity **(Figure 4I-J)**. Having shown that IL-2-induced mTreg expansion and expression of enkephalin alleviates neuropathic pain, we next investigated whether this could be mediated by the δOR, the preferred receptor for enkephalin. In these studies, we co-administered IL-2 and naltrindole, a selective antagonist of the δOR, and observed that IL-2-induced anti-allodynia was abolished **(Figure 4K-L)**. We conclude that mTreg-derived enkephalin is required for suppressing mechanical pain hypersensitivity and that this suppression is mediated by the δOR.

Treg-derived enkephalin is dispensable for immune suppression

Previously, Tregs have been shown to suppress hyperalgesia following nerve injury by suppressing IFN-ɣ-induced primary afferent sensitization[17]. Thus, we hypothesized that a potential mechanism by which Treg-derived enkephalin mediates the suppression of nociceptive thresholds involves modulation of immunological responses. To address this possibility, we tested the nociceptive thresholds of immunodeficient *Rag2*$^{-/-}$ mice which are missing both T and B cells and compared them to immunocompetent littermates. In these studies, we mated *Rag2*$^{+/-}$ mice and were surprised to observe decreased nociceptive thresholds in the *Rag2*$^{-/-}$ offspring compared to their *Rag2*$^{+/+}$ and *Rag2*$^{+/-}$ littermates. This finding suggests that there may be a mechanism of Treg-mediated control of nociceptive thresholds, which is independent of exaggerated lymphocyte-driven inflammation **(Figure 5A)**. Furthermore, consistent with this conclusion, depleting macrophages through liposomal clodronate administration did not reverse the mechanical allodynia observed in female mice deficient in mTreg **(Figure 5B)**[45].

We also used the *Penk*DTR$^{\Delta heme}$ bone marrow chimeric mice to deplete all bone marrow-derived enkephalin lineage cells and assessed their contribution to the regulation of immune responses. Unlike *Foxp3*-DTR mice, we observed no changes in mouse weight or spleen size in *Penk*DTR$^{\Delta heme}$ bone marrow chimeric mice chronically injected with systemic DT **(Figure S5D-E)**. Furthermore, we also did not observe any specific alterations in CD4^{+} T cell cytokine production after nerve injury in the meninges or lymphoid organs. We conclude, therefore that peripheral enkephalin does not contribute to T cell-driven inflammatory responses **(Figure S5F-G)**.

We next investigated the contribution of Treg-derived enkephalin in the regulation of conventional T cell proliferation. We assessed T cell suppression capacity by co-culturing naïve conventional CD4^{+} T cells with either WT *Penk*$^{+/+}$ or *Penk*$^{-/-}$ Tregs. We observed no difference in the suppressive capacity of *Penk*$^{-/-}$ Treg compared to control Tregs **(Figure 5C-D)**. Next, we transplanted equal amounts of CD45.1 *Penk*$^{+/+}$ or CD45.2 *Penk*$^{-/-}$ CD4^{+} T cells into *Rag2*$^{-/-}$ mice and performed SNI to measure chimerism of congenic markers among CD4^{+} T cells. We did not observe a competitive advantage or disadvantage amongst *Penk*$^{-/-}$ CD4^{+} T cells across various tissues **(Figure 5E-G)**. Restimulating harvested T cells from distinct tissues with PMA/Ionomycin revealed no differences in T cell differentiation across Tregs, T helper 1 (Th1) and Th17 subsets between the *Penk*-sufficient or deficient T cells **(Figure 5H and Figure S5H-I)**. In addition, we noticed no difference in weight, health, or spleen size between *Penk*$^{\Delta heme}$ *and WT*$^{\Delta heme}$ bone marrow

321 chimeric mice further revealing that peripheral enkephalin has a very limited, if any, role
322 in the suppressing of systemic inflammatory responses **(Figure S5J-K)**.
323
324 Finally, using an adoptive transfer-based graft versus host disease (GVHD) model, we
325 assessed whether Treg-derived enkephalin is required for suppressing immune
326 responses. As expected, we observed a profound Th1 response in mice transferred with
327 activated Tconv alone. However, mice that received additional transfers of either *Penk*$^{+/+}$
328 or *Penk*$^{-/-}$ Tregs equally suppressed Th1 responses, reduced GVHD severity and
329 mitigated weight dysregulation **(Figure 5 I-J and S5L-N)**. In summary, we conclude that
330 Treg-derived enkephalin does not contribute to any inflammatory response restraint
331 mechanism. Rather, we conclude that Tregs can suppress pain sensitivity through a
332 mechanism that is independent of their function in immunosuppression.
333
334 ***Delta opioid receptor signaling on MrgprD^{+} primary afferent DRG neurons is***
335 ***required for the anti-allodynic function of mTregs***
336 Enkephalin is a potent agonist at the δOR, and, to a lesser extent the μOR. In our previous
337 studies, we demonstrated the divergence of expression and function of δOR and μOR in
338 mediating distinct pain modalities. Specifically, δOR is expressed on nonpeptidergic IB4^{+}
339 unmyelinated as well as myelinated primary afferents and selectively regulates
340 mechanical thresholds and nerve injury-induced mechanical hypersensitivity[21].
341 Conversely, the μOR is expressed on Trpv1^{+} nociceptors and selectively regulates
342 thermal hyperalgesia. In addition, a spinal δOR can dampen mechanical hypersensitivity
343 by inhibiting the excitability of somatostatin-positive dorsal horn interneurons[23].
344
345 To assess the requirement of PNS or CNS δOR circuits in coordinating the anti-allodynic
346 effect of mTregs, we intravenously injected *Oprd1*$^{+/+}$ control or *Oprd1*$^{fl/fl}$ mice with
347 AAV.PHP.S-CAG-Cre or AAV.PHP.eB-CAG-Cre. This approach selectively introduces
348 Cre recombinase and targets deletion of δOR into to the PNS (DRG) or CNS (spinal cord
349 and brain), respectively **(Figure 6A).** Three weeks after the AAV injection, we performed
350 SNI and four weeks later administered IL-2. Mice selectively lacking δOR in the PNS lost
351 the capacity to respond to the anti-allodynic effect of IL-2, but the effects of IL-2 were
352 preserved in mice lacking δOR in the CNS **(Figure 6B-C)**. We conclude that a sensory
353 neuron-expressed, presynaptic δOR coordinates mTreg suppression of mechanical pain
354 hypersensitivity.
355
356 Next, we identified the specific sensory neuron subset that coordinates the anti-
357 nociception mediated by mTreg-derived enkephalin. Previous studies of δOR expression
358 on DRG sensory neurons using *Oprd1*^{eGFP} reporter mice revealed that approximately half
359 of the reporter-positive cells in the DRG are myelinated neurons, while approximately
360 36% are IB4^{+} non-peptidergic neurons expressing the MrgprD receptor. Using
361 established single cell RNA sequencing resources, we found that the MrgprD^{+} subset of
362 DRG sensory neurons not only expresses *Oprd1*, but also other receptors for Treg
363 ligands, including *Il10ra and Icosl*, which have been implicated in suppression of pain
364 thresholds[46–48] **(Figure 6D)**. The total proportion of sensory neurons expressing the
365 *Oprd1* transcript matches previous data using *Oprd1*^{eGFP} reporter mice **(Figure 6E)**. Our
366 subsequent flow cytometry-based profiling of *Oprd1*^{eGFP} reporter expression on DRG cells

367 confirmed GFP expression specifically on IB4$^+$ CD45$^-$ Thy1$^+$ sensory neurons, which
368 corresponds to the MrgprD$^+$ nonpeptidergic nociceptive neuron population. Importantly,
369 the flow analysis confirmed the absence of GFP expression on broadly defined CD45$^+$
370 CD90.2$^+$ IB4$^-$ lymphoid cells and CD45$^+$ CD11b$^+$ CD90.2$^-$ IB4$^-$ myeloid cells **(Figure 6F)**.
371 We also confirmed the absence of GFP expression on microglia as well as on immune
372 cells profiled from the draining lymph nodes (data not shown)[23]. Based on this selective
373 Oprd1 expression profile, we generated mice in which MrgprD$^+$ neurons lack the δOR
374 (*MrgprD*$^{Cre\text{-}ERT2}$;*Oprd1*$^{fl/fl}$). Female *MrgprD*$^{Cre\text{-}ERT2}$*;Oprd1*$^{fl/fl}$ mice, but not their male
375 counterparts, exhibited exaggerated mechanical hypersensitivity after SNI compared to
376 tamoxifen-injected sex-matched littermate controls **(Figure 6G-H)**. Female mice lacking
377 δOR on MrgprD$^+$ sensory neurons and treated with IL-2 IT four weeks following SNI
378 displayed a complete deficiency in IL-2 anti-allodynic efficacy **(Figure 6I-J)**. We conclude
379 that, the enkephalin receptor δOR, expressed specifically by MrgprD$^+$ sensory neurons,
380 mediates the anti-nociceptive function of mTregs.
381
382 ***mTreg expansion promotes pregnancy-induced analgesia***
383 Our studies described above uncovered a sex-selective and hormonally driven regulatory
384 T cell pathway for pain regulation. Here we examined whether this pathway comes into
385 play during pregnancy, a state that is characterized by numerous temporally dependent
386 hormonal changes. Pregnancy-induced analgesia refers to the phenomenon
387 characterized by a decrease in pain sensitivity to an acute stimulus or an improvement in
388 pain associated with pre-existing chronic pain[6,49]. Previous studies in pregnant rats
389 subjected to foot shocks described a mechanism of PIA that is dependent on endogenous
390 opioids and independent of the adrenal gland function[6,50]. In mice, *Oprd1* expression
391 levels increase in the DRG during gestation, and PIA is abolished in immunodeficient
392 *nude* mice[49]. In pregnant women, migraine-associated pain is significantly improved
393 during pregnancy. In fact, a large meta-analysis reported significant improvement or
394 remission of migraine in nearly 50-70% of individuals during pregnancy[4]. Chronic pain
395 syndromes associated with autoimmunity, such as rheumatoid arthritis, also improve due
396 to the improvement of the inflammatory component of the disease during pregnancy[7].
397 Thus, there appears to be a cross-species phenomenon for pain suppression during
398 pregnancy, but the mechanisms are not fully understood.
399
400 To uncover a potential Treg/δOR mechanism of PIA, we mated C57BL/6 WT female mice
401 4 weeks after SNI with a syngeneic male partner. We tracked mechanical thresholds
402 before and throughout pregnancy and after delivery. Before pregnancy, the SNI mice
403 exhibited mechanical sensitivity at the lowest limit of detection of von Frey filaments.
404 Shortly after mating, the pregnant mice displayed gradually increasing mechanical
405 thresholds compared to nerve-injured nulliparous controls. The PIA lasted throughout the
406 full term of the pregnancy, reaching maximal, suprabasal thresholds near the end of
407 gestation **(Figure 7A-B)**. We did not observe increased fetal resorption, decreased litter
408 size or alteration of offspring weight from SNI mice compared to sham controls **(Figure**
409 **S6A-C)**. Strikingly, after delivery, the mechanical thresholds sharply dropped to their pre-
410 mating thresholds and remained at this level unless the mice were mated again. Given
411 the near immediate drop of mechanical thresholds after delivery and observation of PIA
412 in syngeneic mating, we hypothesized that the mechanism of PIA is independent of fetal

antigen-specific maternal T cells. Consistent with this conclusion, we found that IT injection of the δOR antagonist, naltrindole, fully eliminated PIA compared to vehicle-injected pregnant controls **(Figure 7C)**. Furthermore, mice lacking δOR on MrgprD^{+} sensory neurons had a profound absence of PIA compared to their littermate controls **(Figure 7D)**. Taken together, we conclude that PIA is dependent on endogenous δOR signaling in the DRG.

Next, we mated *Rag2*$^{-/-}$ mice with SNI with syngeneic males and uncovered a near-complete loss of PIA during the first 2 trimesters of gestation. Interestingly however, we observed the presence of a lymphocyte-independent analgesic mechanism during late pregnancy **(Figure 7E)**. Administration of deltorphin 2 IT, a δOR selective agonist, into *Rag2*$^{-/-}$ mice during the first two trimesters of pregnancy prompted a robust suppression of mechanical sensitivity **(Figure 7F)**. This result further demonstrates that the δOR anti-nociceptive signaling is downstream of the adaptive immune system.

Finally, we investigated whether mTreg number change during pregnancy. There is, in fact, a substantial literature indicating that systemic Tregs expand during pregnancy in response to fetal antigens, which supports fetal tolerance and pregnancy success[10,16] or to suppress autoimmune diseases[51]. Here, we analyzed Treg expansion in pregnant *Penk*^{Cre}*;Rosa26*^{tdTomato} mice with SNI, at the end of the second trimester of pregnancy when the PIA is maximal. There is indeed a significant increase in mTreg number as well as enkephalin-lineage positive mTregs **(Figure 7G-I)**. Importantly, this increase was not observed for enkephalin fate positive Tregs in the lymphoid organs **(Figure 7J).** Furthermore, depletion of mTregs during pregnancy led to a near-complete loss of PIA in pregnant *Foxp3*-DTR mice with SNI, compared to WT controls injected with pegDT IT **(Figure 7K-L)**. Site specific depletion of mTreg avoided the fetal loss that is observed in the context of systemic Treg ablation **(Figure S6D-E)**[10,16]. We conclude that mTregs expand during gestation and establish pregnancy-induced analgesia through the secretion of endogenous opioid enkephalin in the meninges that acts on δOR on MrgprD^{+} sensory neurons. These findings elucidate a sex-selective, analgesic function of regulatory T cells that may have evolved to modulate sensory input and behaviors and importantly to sustain pregnancy perseverance.

Discussion

In this report, we describe a novel, sexually dimorphic mechanism for pain regulation by the immune system. Using a host of site-selective targeting strategies to deplete or expand Tregs within the recently appreciated borders of the nervous system, namely the meninges, we find that mTregs can profoundly gate mechanical hypersensitivity. Strikingly, this pain regulatory function of mTregs is sex-specific and under the control of gonadal hormones. Expression of proenkephalin by Tregs has been incidentally reported in sequencing studies but the functional relevance of those findings was never established. Here we demonstrate that mTreg-secreted enkephalin acts on primary sensory neuronal δOR to selectively modulate mechanical sensitivity. In pregnancy, enkephalinergic mTregs expand and promote analgesia in a pre-existing neuropathic pain condition. Our findings not only provide the first mechanism of pregnancy-induced analgesia, but also distinctively augment the current understanding of pregnancy-protective functions of Tregs and establishes regulatory T cells as sentinels of pain homeostasis.

To assess for sex differences in transcriptional identify after nerve injury, primary afferent neurons, including those expressing MrgprD, have recently been sorted for deep RNA sequencing[52]. Surprisingly, very few differences were found between the sexes, suggesting a lack of a strong intersection of sex and injury in the transcriptional identity of peripheral neurons. The lack of transcriptional differences may also suggest that non-neuronal cells may be a primary determinant of sex-selective pain modulation. Indeed, preclinical research has demonstrated the involvement of T cells in driving pain phenotypes in female mice[53]. Additionally, human leukocyte antigen (HLA) risk alleles have been identified for human chronic pain conditions, further suggesting a potential role for T cells in pain modulation[24,54].

Regulatory T cells display broad tissue supportive roles that extend beyond their originally described function in suppressing inflammation[8,11,12,20]. A major advantage of our analysis is that we utilized a site-selective mTreg ablation strategy that preserved peripheral Tregs and avoided systemic inflammation. Using this approach, we identify a novel, sex-specific mechanism by which Tregs modulate nociceptor activity to regulate pain sensitivity in the context of health and nerve injury. Although, proenkephalin-expressing Tregs have been identified in various tissues, their functional assessment has been limited[19,37,38]. Somewhat paradoxically, a recent pre-print study demonstrated a small but statistically significant decrease in basal heat sensitivity in both female and male mice conditionally depleted for *Penk* expression in systemic Tregs. Mechanical thresholds and other sensory modalities were however not examined[55]. In distinct contrast, we uncover a sensory modality selective function of mTreg that is consistent with prior findings of δOR agonism, namely providing relief of mechanical but not heat pain[21,56]. Whether mTregs tonically restrain nociception is difficult to conclude. Our finding of increased basal sensitivity in *Rag2*$^{-/-}$ or *Penk*$^{\Delta heme}$ mice, is supportive of this hypothesis, however, alternative possibilities exist. It is conceivable that mTreg deficiency could lead to inflammation, which may alter nociceptor sensitivity. Additionally, the endogenous opioid signaling pathway may have a role in opioid induced analgesia. It is significant that naloxone, a non-selective opioid receptor antagonist IV injection, does not induce pain in

healthy individuals. Whether experiments in uninjured female mice have been performed is unclear[57].

Our observations suggest that sex hormones, not sex chromosomes, are the main drivers of mTreg-induced anti-nociception, a conclusion confirmed by our finding that gestation induces mTreg expansion to promote pregnancy-induced analgesia. Which specific sex hormones regulate mTreg function in pain is still unclear, but prior studies have implicated estrogen and progesterone in regulating neuropathic pain associated with SNI[49]. Estrogen administration increases *Penk* expression in the whole spinal cord[58]. Moreover, in $CD4^+$ T cells, the estrogen receptor engages conserved non-coding sequences (CNS) in *Foxp3* enhancer regions[59]. Importantly, *Foxp3* CNS regions are conserved selectively in placental mammals and play a role in extrathymic Treg generation to preserve pregnancy by promoting maternal-fetal tolerance[10]. As PIA sharply diminishes after delivery and develops during syngeneic pregnancies, we suspect that Treg-mediated PIA is fetal antigen-independent. It will be interesting to determine whether mothers would experience heightened PIA during subsequent pregnancies or following allogenic mating. Finally, pregnancy-induced reversal of allodynia amidst chronic, non-healing neuropathic injury, illuminates a remarkable ability within nociceptors to finely tune noxious sensory input depending on the physiological context.

Methods

Mice

All mouse experiments were approved by UCSF Institutional Animal Care and Use Committee and conducted in accordance with the guidelines established by the Institutional Animal Care and Use Committee and Laboratory Animal Resource Center. All mice experiments were performed on age-matched adult male and female mice at a starting age between 8 and 14 weeks old. Littermate controls were used for all experiments when feasible. Mice were bred in-house and backcrossed over 10 generations to C56BL/6 breeders obtained from Jackson labs. Experimental mice were co-housed to maintain the same microbiome. They were maintained in a temperature (21°C) - and light (12h light/dark cycle)-controlled environment and were provided with food and water *ad libidum*. The following mouse strains are used: C57BL/6J (JAX #000664), *Foxp3*-DTR (B6.129(Cg)-Foxp3tm3 (Hbegf/GFP)Ayr/J, JAX# 016958), *Foxp3*$^{eGFP\text{-}Cre\text{-}ERT2}$ (Foxp3tm9 (EGFP/cre/ERT2)Ayr/J; JAX#016961), Ai9 (B6.Cg-*Gt(ROSA)26Sor*$^{tm14(CAG\text{-}tdTomato)Hze}$/J; JAX#007914), Four Core Genotypes (B6.Cg-Tg(Sry)2Ei Srydl1Rlb T(XTmsb4x-Hccs;Y)1Dto/ArnoJ; JAX#010905), Penk-IRES2-Cre(B6;129S-Penktm2(cre)Hze/J; JAX#025112), Rosa26-ISL-iDTR (CBy.B6-Gt(ROSA)26Sortm1(HBEGF)Awai/J;JAX#008040),CD45.1 (B6.SJL-Ptprca Pepcb/BoyJ; JAX# 002014), B6C3F1/J (JAX#100010), *Rag2*$^{-/-}$ (B6.Cg-Rag2tm1.1Cgn/J; JAX#008449), Mrgprd-CreERT2 (Mrgprdtm1.1(cre/ERT2)Wql/J; JAX# 031286), Oprd1fl/fl (B6;129-Oprd1tm1.1Cgrf/KffJ; JAX# 030075), DOR-eGFP (B6;129S2-Oprd1tm2Kff/J; JAX#029012). *Penk*$^{-/-}$ were kindly provided by Dr. John Pintar on a C57BL/6 background (MGI 3628668)[60]. *Foxp3*-DTR (X-linked) was mated with male Four Core Genotypes XY$^{Sry\text{-}}$Sry^{Tg} and the X$^{Foxp3\text{-}DTRYSry\text{-}}$Sry^{Tg} male mice were mated to homozygous *Foxp3*-DTR female mice.

Pregnancy model

Mice were harem bred (2-4 females) with a single male breeder 4 weeks after nerve injury. Female mice were checked daily after mating and behavior measurements were started after copulatory plugs were observed in females (around 3-4 days). Male breeders were housed with the female for the duration of the experiments. Females were tested every three days for pregnancy-induced analgesia. Late pregnant females were checked daily for delivery and results were plotted based on the delivery date. Pregnancy-induced analgesia started approximately 1-3 days after copulation plug was observed and given the variability in gestation duration from 18-21 days, the last 18 days of pregnancy was plotted to standardize the curve. Area under the curve was calculated for paw withdrawal thresholds in respect to time.

Bone marrow transplantation

CD45 mismatched host recipient mice were irradiated at 550 cGy twice, 5 hours apart and injected retro-orbitally with $5x10^6$ cells from the bone marrow of CD45.1 WT, *Penk*^{Cre};*Rosa26*^{DTR} *Penk*$^{-/-}$ or a 1:1 mix of *Foxp3*-DTR and *Penk*$^{-/-}$ sex-matched 7-10 week old mice. Mice were kept on doxycycline chow for the first week (Bioserv #S3888) and chimerism was assessed at 8 weeks post-transplant.

Pharmacological interventions

Animals were randomly assigned to vehicle control or treatment group. Pegylated diphtheria toxin (pegDT) was a generous gift from Ana I. Domingos and generated as previously described[61]. pegDT (20 ng) or corresponding phosphate-buffered saline (PBS) control were injected intrathecally (IT) in a volume of 5μL in naive mice below lumbar level L4. All intrathecal injections were performed in non-anesthetized, lightly restrained mice and injections were validated by a sudden flick of the tail. Of note, the 5-10 μL injection distributes predominantly to the lumbo-sacral cord given lidocaine IT injection at that segment paralyzes the hindpaws but not forepaws. For pregnancy experiments, pegDT (40 ng IT) was administered two days before mating, and every subsequent four days until delivery. Non-pegylated diphtheria toxin (30 ng/g, Sigma Cat#322326) or corresponding saline control were administered in a volume of 200 μl every three days intraperitoneally (IP). IL-2 (0.1 μg, Peprotech, Cat# 212-12) or PBS vehicle control were administered daily for three consecutive days IT. Selective δOR agonist, [D-Ala2]-Deltorphin 2 (15 μg, Abcam Cat #ab120708, CAS 122752-16-3) and selective δOR antagonist, naltrindole (5 μg, Sigma Cat# N115) administrations were performed 30 min before behavior experiments. For pregnancy-induced analgesia experiments, naltrindole was administered IT every three days, throughout pregnancy and Deltorphin 2 was administered three times in the two first trimesters of pregnancy.

Tamoxifen injections

Mrgprd$^{\text{CreERT2}}$;*Oprd1*$^{\text{fl/fl}}$ and *Foxp3*$^{\text{eGFP-Cre-ERT2}}$;*Rosa26*^{tdTomato} mice were injected IP with tamoxifen (Sigma Cat #5648) 100 mg/kg in corn oil (Sigma Cat #8267) for five consecutive days to induce Cre-mediated recombination.

Intrathecal dye tracing

Naive mice were intrathecally injected with 5μL of Evans Blue 1% solution (Sigma, Cat #E2129) or pegylated DyLight 650-4xPEG NHS Ester (Thermo Fischer, Cat #62274). 24 hours post-injection, mice were anesthetized with avertin and euthanized by decapitation. Spinal cord and brain meninges, spinal cord, brain, dorsal root ganglia and trigeminal ganglia, sciatic nerve and lymph nodes were assessed for dye uptake.

Animal behavior

For all behavioral tests, the experimenter was blind to genotype and treatment and performed during the light cycle. For some experiments such as those investigating pregnancy, blinding was not possible. The project utilized both male and female experimenters but a predominant number of experiments were performed by a female investigator[62].

von Frey measurement of mechanical hypersensitivity

Mice were acclimatized once to the von Frey apparatus for two hours. The lateral plantar surface of the ipsilateral and contralateral hind paws (sural innervation) was stimulated with von Frey hairs of logarithmically increasing stiffness (Stoelting Cat # 58011). Animals were habituated on a wire mesh for 1 hour, after which they were tested with von Frey filaments (0.008, 0.02, 0.04, 0.07, 0.16, 0.4, 0.6, 1, 1.4, 2, 4 and 8 g) using the Dixon up–down method[63,64]. The von Frey hairs were held for 3 sec with intervals of several minutes

643 between each stimulation. For the Dixon up-down method we recorded 2 days of baseline
644 mechanical sensitivity which were averaged. After SNI, nearly all mice reached a 50%
645 paw withdrawal threshold of the lowest filament (0.008 g), thus we utilized a single fiber
646 method of testing to achieve resolution of allodynia severity. Mice were stimulated 10
647 times with the 0.008 g filament. The filament was applied for 3 seconds and the number
648 of positive responses across the 10 stimulations were registered as percent nociceptive
649 responses.
650
651 **Hargreaves measurement of heat hypersensitivity**
652 Mice were acclimatized for 30 min in plexiglass cylinders. The mice were then placed on
653 the glass of a Hargreaves apparatus and the latency to withdraw the paw from the heat
654 source was recorded. Each paw was tested three times and latencies were averaged
655 over the trials.
656
657 **Acetone induced cold sensitivity**
658 Mice were habituated for 60 min on a mesh in plexiglass cylinders. A syringe was used
659 to spray 50 µl of acetone (Thermo Scientific Cat # 423240010) onto the plantar surface
660 of the paw and the behaviors were video recorded for 30 seconds after each trial using a
661 Sony HDR-CX440 camera. The left hind paw was tested five times and positive
662 responses included withdrawals, shakes, licks and jumps. Results are displayed as the
663 total number of behaviors across the five trials.
664
665 **Tail flick measurement of heat hypersensitivity**
666 Mice were placed in a restrainer and 2 cm of the tip of the tail was submerged in a 52°C
667 water bath. The latency (seconds) to withdraw the tail from the water was recorded. A
668 cut-off of 15 s was set to prevent tissue damage and testing was performed with intervals
669 of several minutes between each stimulation. Mice were tested three times and
670 withdrawal latencies were averaged.
671
672 **Hot plate measurement of heat hypersensitivity**
673 Mice were acclimated to the testing environment as described above. The hot plate
674 temperature was set to 52°C. The mouse was placed on the plate and the latency to
675 shake, lick or bite a hindpaw was scored. A cut-off of 20 s was set to prevent tissue
676 damage.
677
678 **Pin prick withdrawal test**
679 Mice were habituated for 60 min on a mesh in plexiglass cylinders. A 27G needle was
680 gentle applied onto the hindpaws, with minutes between each stimulation for a total of 5
681 stimulations per paw. Mice were scored as follow: 1: brief withdrawal, 2: mice lifting their
682 paw for 1 sec, 3: mice lifting their paw for 2 sec or shake, 4: lick. Results are displayed
683 as the total number of behaviors across the five trials.
684
685 **Brush withdrawal test**
686 Mice were habituated for 60 min on a mesh in plexiglass cylinders. A 5-0 brush was gently
687 applied onto the hindpaws, with minutes between each stimulation for a total of 5
688 stimulations per paw. Mice were scored as follow: 1: brief withdrawal, 2: mice lifting their

689 paw for 1 sec, 3: mice lifting their paw for 2 sec or shake, 4: lick. Results are displayed
690 as the total number of behaviors across the five trials.
691
692 **Rotarod**
693 Mice were acclimatized to the testing room and trained by placing them on an accelerating
694 rotarod for a maximum of 60 seconds at low speed, three times with training taking place
695 on two consecutive days. Latency to fall was measured with a cutoff of 300 seconds. The
696 procedure was repeated three times and latencies averaged across trials.
697
698 **Spared Nerve injury**
699 We employed an established, robust and reliable spared nerve injury (SNI) model to
700 induce a chronic neuropathic injury[65]. This model utilizes non-healing surgical intervention
701 on two branches of the sciatic nerve (the common peroneal and tibial branches), while
702 sparing the third branch (the sural branch) for sensory testing on the lateral portion of the
703 hindpaw. Briefly, mice were anesthetized with isoflurane (3% for induction and 1.5% for
704 maintenance, mixed with oxygen). The fur on the left hind leg was shaved and disinfected
705 with 3 passages of alcohol and iodine solution, alternatively. A 1 cm incision was
706 performed on the upper thigh skin, near the division point of the sciatic nerve. A 2%
707 lidocaine solution was applied and the biceps femoris muscle was gently separated
708 through a blunt opening to reveal the sciatic nerve's common peroneal, tibial, and sural
709 branches. The common peroneal and tibial nerves were ligated with non-dissolvable 8-0
710 silk sutures (Fine Science Tools Cat # 12052-08). Subsequently, a 2 mm segment from
711 both the common peroneal and tibial nerves was transected, ensuring the sural nerve
712 remained undisturbed. The muscle and the skin were stitched using 6–0 sutures (Henry
713 Schein Surgical suture Cat #101-2636), and the skin was further sealed with a tissue
714 adhesive (3M Vetbond Cat # 1469SB), after an ethanol solution application. Mice were
715 kept on heating pad until they regained consciousness and demonstrated stable,
716 balanced locomotion. Mice were transferred into their home cage and observed
717 meticulously for the next two days.
718
719 **Immunohistochemistry**
720 Avertin-anesthetized mice were transcardially perfused with 10 ml of 1× PBS followed by
721 30 ml of 4% paraformaldehyde (PFA, Thermo Scientific Cat # 119690010) diluted in PBS.
722 After perfusion, spinal cord, sciatic nerves, lymph nodes, spleens, brains and DRG were
723 collected, postfixed in 4% PFA solution at 4°C for 5 h and then cryoprotected in 30%
724 sucrose in PBS at 4°C.
725
726 Spinal meninges were harvested from fixed spinal cords. Spinal cords were transferred
727 in PBS and meninges were gently peeled into a single sheet onto a microscope slide after
728 a longitudinal hemisection of the spinal cord. Brain meninges were similarly harvested
729 from the skull. Frozen tissues were embedded at −35°C in O.C.T. compound and 30 µm
730 transverse spinal cord sections were generated using a Leica SM220R sliding microtome
731 and 20 µm DRG sections were generated using a cryostat (Thermo Fisher Scientific) on
732 SuperFrost Plus slides. Spinal cord sections were processed as free-floating. Sections
733 were blocked (10% NGS, 1% BSA, 0.05% Tween-20, 0.1% Triton X-100 in PBS) and
734 incubated in 0.3 M glycine containing 0.2% Tween 20. Sections were labeled in blocking

buffer for 24 hours at 4°C. Slides were coverslipped with Fluoromount-G (Thermo Fisher Scientific). Fluorescence images were acquired using an Olympus FV3000 confocal microscope and quantified using ImageJ (Fiji).

Tissue clearing

Whole DRG or spinal cords from *Foxp3*$^{eGFP\text{-}Cre\text{-}ERT2}$;Ai9 mice were cleared after PFA fixation using SHIELD tissue clearing (LifeCanvas PCK-500)[66]. Tissues were washed in PBS then processed as previously described[66]. Briefly, the tissues were incubated in epoxy solution (SHIELD OFF) for 10 hours at 4°C with gentle shaking then incubated overnight at 37°C in SHIELD ON-Epoxy solution for epoxy crosslinking. DRG were then further incubated in SHIELD ON solution for 10h and delipidated for two days (DRG) to five days (spinal cord) at 45°C with shaking then washed with PBS. Whole mount DRG and spinal cords were acquired in FocusClear reflexive index matching solution (CelExplorer, FC-102).

Tissue digestion

Mice were injected intravenously with 50 µl of anti-ARTC2 nanobody (Biolegend Cat # 149802) in 200 µL of PBS 30 minutes before euthanasia to protect Treg during harvest from purinergic-mediated cell death[67]. 5 minutes before harvest mice were injected intravenously with 6 µg of FITC-conjugated anti-CD45 antibody to label blood immune cells in 200 µL of PBS [27]. Avertin-anesthetized mice were decapitated, and spinal cord meninges, brain meninges, L4-6 DRG, sciatic nerves, lymph nodes, brains and spleens were harvested. Spinal cord meninges, brain meninges, DRG, sciatic nerves and brains were crushed with the back of a 3ml syringe in a serrated 24 well plate and triturated in digestion media (Liberase TM (0.208 WU/ml) (Roche Cat # 054010200001) and DNase I (40 ug/ml) (Sigma Cat # DN25) in 1.0 ml cRPMI (RPMI supplemented with 10% (vol/vol) fetal bovine serum (FBS), 1% (vol/vol) HEPES, 1% (vol/vol) Sodium Pyruvate, 1% (vol/vol) penicillin-streptomycin). They were digested for 30 min at 37°C, 220 RPM and triturated every 15 minutes. Digested samples were again triturated and passed over a 40 µm cell strainer and any remaining tissue pieces mashed through the cell strainer. Cell strainers were flushed with staining media (PBS w/o Mg^{2+} and Ca^{2+} supplemented with 3% FBS, 2 mM EDTA and 0.05% NaN_3). Single-cell suspensions were centrifuged at 500 g at 4°C, washed and resuspended in staining media. Spleens and lymph node immune cells were obtained by mashing the tissues over a 40 µm cell strainer and washed with staining media.

Cell stimulation

Isolated single cell suspensions were incubated for 4 hr at 37°C in complete IMDM (supplemented with 10% FBS, 2 mM L-glutamine, 10 mM HEPES, 1% sodium pyruvate, 1% penicillin-streptomycin, 50 µM 2-mercaptoethanol) with (phorbol 12-myristate 13-acetate) PMA, Ionomycin in the presence of Brefeldin A and Monensin (Tonbo, TNB-4975).

781 **Flow cytometry**
782 Single-cell suspensions were stained in a 96 well plate. Briefly, they were washed with
783 250 µL of staining media and stained with viability dye (1:500) and cell surface antibodies
784 (1:100) in 100 µL of staining media with Fc shield (1:100). Samples were washed twice
785 in staining media and stained for intracellular cytokines or for Foxp3 according to
786 manufacturer recommendations with BD Cytofix/Cytoperm Fixation/Permeabilization Kit
787 (BD 554714, AB_2869008). Samples were further stained with conjugated intracellular
788 antibodies (1:100) overnight at 4°C in BD permeabilization/wash buffer. Samples were
789 washed with permeabilization/wash buffer twice and resuspended in 200 µL of staining
790 media. For visualization of both tdTomato reporter signal and intranuclear Foxp3 signal,
791 cells were fixed in 200 µL of freshly prepared 2% formaldehyde (EM grade) in PBS for 60
792 minutes exactly and washed with eBioscience Permeabilization buffer (eBioscience
793 Foxp3 perm-kit) and stained overnight in 1x eBioscience Permeabilization buffer at 4°C[68].
794 Cells were washed twice in the buffer and resuspended in staining media. For Met-
795 enkephalin staining, we screened multiple commercially available antibodies and
796 selected an antibody that showed positive staining in wildtype mTreg but not *Penk*$^{-/-}$
797 mTreg. The antibody was conjugated to fluorescent phycoerythrin with Lightning-link
798 conjugation kit (ab102918) and utilized after cell stimulation and intracellular cytokine
799 staining. Cells were counted with 50 µL of counting beads (Thermo Fisher Scientific Cat
800 # C36950) and samples were analyzed using a BD FACSCanto2 or BD FACS Aria Fusion
801 flow cytometer (BD Biosciences). Positive and negative selection gates were set using
802 fluorescence minus unstained cells. For negative control of enkephalin staining, *Penk*$^{-/-}$
803 samples were used for gating. Fluorescence intensity distribution was analyzed using
804 FlowJo 10 software (BD Biosciences). Antibodies for flow cytometry are listed in the
805 resource table. Lineage exclusion markers include viability dye, CD11b (to exclude
806 myeloid cells), B220 (to exclude B cells), Ter119 (to exclude red blood cells).
807
808 **Cell sorting**
809 Spleens were mashed on a cell strainer and cells were pelleted at 500 g for 10 min at
810 4°C. Cells were stained for viability and lineage exclusion markers, in addition to CD45,
811 CD4, CD45RB to stain naïve Tconv and CD25 to stain Tregs. Cells were pelleted, washed
812 and incubated with CD4 negative selection beads and purified on a LS magnetic column
813 (Miltenyi Biotec). Cells were double sorted in BD FACS Aria Fusion for Singlet, Live,
814 CD45$^+$ CD4$^+$ CD45RB$^+$ CD25$^-$ for Tconv or Singlet, Live, CD45$^+$ CD4$^+$ CD25$^+$ CD45RB$^-$
815 for Treg into complete IMDM.
816
817 **T cell suppression assay**
818 Sorted Tconv from lymphoid organs of CD45.1 female mice were labeled with cell trace
819 violet (Thermo-Fisher, Scientific #C34571) according to manufacturer instructions.
820 0.25×10^5 Tconv per well were cultured with distinct dilution of Treg from CD45.2 WT or
821 *Penk* deficient lymphoid organs. Cells were then washed and resuspended with mouse
822 anti-CD3/CD28 Dynabeads at a 1:1 ratio of beads to Tconv. Cells were incubated for 96
823 hours in a humidified incubator at 37°C. Cells were washed and resuspended in staining
824 media and suppression ratio was calculated by dividing the percent proliferated cells from
825 incubated Tconv$^+$ Treg samples by percent proliferated cells from Tconv only samples[69].
826

827 **T cell adoptive transfer**
828 *Competition assay*
829 1x10^6 negatively selected bulk $CD4^+$ T cells from WT female and *Penk* deficient lymphoid
830 organs were transplanted into female *Rag2*$^{-/-}$ mice. SNI was performed and organs were
831 collected 28 days later for cell stimulation and flow cytometry.
832
833 *Graft versus host disease (GVHD)*
834 GVHD was established as previously described. Briefly, WT or *Penk* deficient female
835 mice bone marrow was transplanted into MHC mismatched B6C3F1/J female mice to
836 activate T cells. 0.25x10^6 sorted WT Tconv were transplanted into male *Rag2*$^{-/-}$ mice to
837 induce chronic GVHD either without Tregs or in the presence of 0.125 x10^6 WT or *Penk*
838 deficient Tregs. Mice were measured for weight changes and GVHD score. Mice were
839 euthanized then harvested for cytokine secretion assay by flow cytometry[70,71]. GVHD
840 scoring is as follows: 0 = no signs of GVHD, 1 = visible signs of GVHD (hunching, lethargy,
841 ruffled fur), 2 = no weight gain, 3 = 0-5% weight loss, 4 = >5% weight loss. One Tconv
842 mouse did not survive for harvesting for cytokine stimulation.
843
844 *Pregnancy*
845 28 days post SNI Female *Rag2*$^{-/-}$ mice were transplanted intravenously with 5x10^6
846 negatively selected bulk $CD4^+$ T cells from female WT and *Penk* deficient mice. Mice were
847 mated and assessed for change in nociceptive thresholds.
848
849 **Analysis of sequencing data**
850 *Bulk RNA-seq*
851 Raw files GSM4677053-064 from GEO dataset GSE154680, and all files from GSE
852 GSE180020 were gathered and aligned using STAR for uniquely mapped reads
853 (outFilterMultimapNmax 1–outFilterMatchNmin 30–alignIntronMin 20–alignIntronMax 1-
854 0000). Data was annotated with GENCODE GRCm38/mm10 genome assembly. Raw
855 count tables were normalized by median of ratios method with DESeq2 package from
856 Bioconductor to analyze for differential expression.
857
858 *ATAC-seq*
859 Fastq files were gathered from SRR12264679-94 from GSE154680. Raw reads were
860 mapped to the mouse mm10 genome assembly using STAR alignment (--
861 outFilterMismatchNoverLmax 0.04 --outFilterMismatchNmax 999 --
862 alignSJDBoverhangMin 1 --outFilterMultimapNmax 1 --alignIntronMin 20 --
863 alignIntronMax 1000000 --alignMatesGapMax 1000000). Bam files were generated by
864 STAR. PCR duplicates were removed by Picard, and peak calling performed using
865 MACS2 (--keep-dup 1 --bw 500 -n output --nomodel --extsize 400 --slocal 5000 --llocal
866 100000 -q 0.01) PMID: 22936215). To generate bigwig files for ATAC-seq datasets, all
867 aligned bam files were merged by condition using samtools merge. Bedtools genomecov
868 was run to covert the merged bam files into a bedgraph files. Finally, bedGraphToBigWig
869 (ucsc-tools/363) was used to generate the bigwig files displayed on browser tracks using
870 the IGV browser and compared to existing encode ATAC and Chip-Seq peaks.
871
872

scRNA-seq

Fastq files were gathered from GEO from datasets GSE139088 GSE201653 and initial counts were obtained using the Cell Ranger pipeline[48,72]. Using Seurat v4, individual cells were removed from the data set if they had fewer than 1000 discovered genes/features, fewer than 1000 UMI or greater than 10% reads mapping to mitochondrial genes. 2000 variable genes were found for each normalized library, and anchors were selected for integration with dimensionality of each dataset set at 30. Glial cells noted for the markers of *Sparc* and *Mpz* and non-neuronal cells lacking the expression of Avil were excluded. Variable genes were identified from the merged dataset, and PCA and UMAP were ran to generate new UMAP coordinates with a dimensionality of 30 and clustering was performed with a resolution of 0.5. Findallmarkers function utilizing a Wilcoxon rank-sum test was used to find cluster specific markers and annotation was performed as recently established[48]. Number of *Oprd1* expressing cells were defined by a threshold of non-zero expression.

Statistical analysis

Statistical analysis was performed using GraphPad Prism 9 software. Data are presented as mean ± SEM. Differences pre- and post-injection within a single group were assessed using a Wilcoxon matched-pairs signed rank test. Differences between two groups were assessed using a Mann-Whitney test. Statistical analysis for multiple comparisons were performed using Kruskal-Wallis test followed by Dunn's multiple comparison test or a Two-Way ANOVA followed by Sidak's multiple comparison test. $p < 0.05$ (*), $p < 0.01$ (**), $p < 0.001$ (***).

Acknowledgement: We thank Dr. Dena Dubal and her laboratory for the FCG mouse, Dr. Kevin Yackle for *Penk*^{Cre} mice, Dr. Ari Molofsky for *Foxp3*$^{Cre\text{-}ERT2}$*Rosa26*^{TdTomato} mice, Dr. Amynah Pradhan for *Oprd1*^{eGFP} mice and Dr. Mike Ansonoff for assistance with Penk$^{-/-}$ tissue isolation. We thank additional members of the Basbaum laboratory and UCSF ImmunoX for critical feedback. Funding for this work was supported by grants Canadian Institute of Health Research (CIHR) (to É.M.), the Fonds de Recherche en Santé-Québec (to É.M.), the Dermatology Foundation (Career Development Award to S.W.K.), the Sandler Foundation PBBR (to S.W.K), Grunfeld Scholar Award from SFVAMC (to S.W.K), T32AR007175-44 (to S.W.K), NIH NSR35NS097306 (to A.I.B.) and Open Philanthropy (to A.I.B.). Figures were generated with BioRender.com.

Disclosures: Authors have no conflicts of interests to declare.

Author contributions: É.M. and S.W.K. designed experiments. É.M., B.C.M, J.B., S.R. N.P.K. W.L.E. and S.W.K. performed experiments, data analysis or visualization. J.E.P. and A.I.D. provided critical reagents or tools. S.W.K, É.M. and A.I.B., acquired funding and provided supervision. É.M, A.I.B and S.W.K. wrote the manuscript.

Material availability and requests: No new reagents, original code or original genomic datasets were generated. Requests for reagents or mice can be sent to sakeen.kashem@ucsf.edu or allan.basbaum@ucsf.edu.

Diversity, equity, and inclusion statement: Authors support diversity and inclusion values. At least one author, including the lead author, self-identifies as a woman. At least one author identifies as an under-represented minority and/or as an immigrant.

Figure Legends

Figure 1. mTreg suppress mechanical pain hypersensitivity in female mice. Representative whole mount maximum projection confocal microscopy image of the (A) lumbar spinal cord meninges and (B) DRG showing Tregs (green-red: yellow) and nerves (autofluorescence, red) in *Foxp3*$^{eGFP\text{-}CreERT2}$*;Rosa26*^{tdTomato} reporter mice. Inlet showing DRG magnification. Scale bar represents 100 µm in A) and 150 µm in B). Arrows indicate Tregs. (C) Total number of weight-adjusted tissue Tregs across organs, in both sexes combined. (D) Relative number of tissue Tregs from male (white) and female (black) mice per organ. 100% represents mean number of female Tregs per organ. Comparison is made between each individual organ. (E) Representative concatenated flow cytometry plots of tissue Treg after a single intrathecal (IT) injection of 20 ng of pegylated diphtheria toxin (pegDT). (F) Relative quantifications of tissue Treg depletion 2 days after a single IT pegDT injection across organs. 100% represents mean number of tissue Tregs in IT vehicle-injected mice per organ. (G and H) 50% paw withdrawal thresholds measured using von Frey filaments before (day 0) and after a single dose of 20 ng of IT pegDT or vehicle in female (G) or male (H) *Foxp3*-DTR mice. (I) Summary of significant behavioral differences comparing IT pegDT- and control-injected female and male mice. Total number of mice for G-I is presented in Figure S3. ScMg= Spinal cord meninges, BrMg= Brain meninges, LN= Lymph nodes, ns = not significant, *p<0.05, **p<0.01, ***p<0.001. **Related to Figure S1-S3.**

Figure 2. Expanding mTreg alleviates nociception dependent on sex hormones and independent of tissue repair.
(A) Schematic representation of the spared nerve injury (SNI) surgery. (B) Long-term assessment of mechanical thresholds in mice following SNI surgery (both sexes combined, no difference between the sexes). n = 7-8 mice per group. (C and D) Percent response to 0.008 g von Frey filament in mice with SNI (day 0) and treated with IT pegDT or vehicle every 4 days. n = 8 per group for females and 9-10 per group for males. (E) Schematic representation of mTreg expansion in mice 4 weeks after SNI by 3 IT injections of low-dose IL-2 (0.1 µg). (F) Total mTreg number in meninges after low-dose IL-2 or vehicle IT injections (both sexes combined, no differences between the sexes). (G and H) Nociceptive thresholds of females (G) and male (H) mice given low-dose IL-2 or vehicle IT 4 weeks after SNI. (I) Schematic representation of the mating strategy of Four Core Genotypes (FCG) *FoxP3*-DTR mice demonstrating resulting XX and XY females and XX and XY male mice. (J and K) Nociceptive thresholds of FCG female (J) and male (K) mice following low-dose IL-2 or vehicle IT injections 4 weeks after SNI. (L) Anti-nociceptive efficacy determined as post IL-2/vehicle injection threshold divided by baseline mechanical threshold in male and female mice with XX (white) or XY (pink) chromosomes. (M) Nociceptive thresholds of FCG *FoxP3*-DTR female and male mice following a single IT pegDT or vehicle injection. (N) Percent baseline nociceptive thresholds determined as post pegDT/vehicle injection threshold divided by baseline mechanical threshold in male and female mice with XX (white) or XY (pink) chromosomes. ns = not significant, *p<0.05, **p<0.01,***p<0.001. **Related to Figure S4.**

1011 **Figure 3. mTregs express and produce enkephalin.**
1012 (A) Volcano plot of transcription fold change of activated Treg (aTreg) vs resting Treg
1013 (rTreg) and (B) heatmap of relative log2 expression value of aTreg, rTreg and activated
1014 and resting $CD4^+$ $CD25^-$ conventional T cells (aTconv and rTconv) from public dataset
1015 GSE154680 (n=3). (C) Averaged ATAC sequencing (ATACseq) of open chromatin
1016 accessibility peaks on the *Penk* locus in different T cell subsets (n=4 per group,
1017 GSE154680), compared to ATACseq, and histone modification Chip-Seq from public
1018 ENCODE dataset of the p0 developing forebrain, a known enkephalinergic region. (D and
1019 E) Log2 values of *Penk* expression by different unstimulated immune cell types from
1020 Immgen dataset GSE180020. (E) Treg *Penk* expression fold change after cytokine
1021 stimulation compared to vehicle control. (F) Representative PMA:Ionomycin stimulated
1022 mTregs, meningeal $CD4^+$ T cells (mCD4) from WT mice or *Penk*$^{-/-}$ mTreg (control). (G)
1023 Representative flow cytometry plots of Tregs from meninges or secondary lymphoid
1024 organs (SLO) from *Penk*^{Cre}*Rosa*26^{tdtomato} mice. Pink represents non-vascular, tissue
1025 Tregs from transgenic *Penk* lineage reporter mice. Gray represents vascular Treg in
1026 reporter mice while Blue corresponds to tissue Treg from non-transgenic control mice.
1027 (H-I) Number of enkephalin lineage fate reporter positive tissue Tregs in (H) meninges
1028 and (I) secondary lymphoid organs (SLO) in male and female mice. NK: Natural Killer
1029 cells, Tgd: γδ T cells, Mo: Monocytes, MF.rp: Red pulp macrophages, CD4T: $CD4^+$ T
1030 cells, CD8T: $CD8^+$ T cells, B.fo: splenic follicular B cells, DC8: $CD8^+$ dendritic cells, pDC:
1031 splenic plasmacytoid, MF.pc: peritoneal macrophages, MC: myeloid cells, B.mz: splenic
1032 marginal zone B cells, ns = not significant, *p<0.05, **p<0.01,***p<0.001.
1033
1034 **Figure 4. mTreg-derived enkephalin controls nociceptive thresholds.**
1035 (A) Representative flow cytometry plots of Cre positive (pink) or Cre negative (blue)
1036 $CD45^+$ non-vascular cells from the meninges and the DRG, combined, from
1037 *Penk*^{Cre}*Rosa26*^{tdTomato} mice. (B) Flow plot shows representative tdTomato negative and
1038 right plot shows tdTomato positive leukocytes, demonstrating the more pronounced
1039 mTreg representation in the enkephalinergic fate cell population. (C) Schematic
1040 representation of bone marrow transplants to generate a global depletion of
1041 enkephalinergic cells, a depletion of hematopoietic-derived enkephalin or a depletion of
1042 Treg-derived enkephalin, respectively. (D-G) Bone marrow chimera of *Penk*^{Cre}*Rosa26*^{DTR}
1043 → irradiated WT recipients. Nociceptive thresholds after a single pegDT (pink) or vehicle
1044 (white) IT injection in female (D) and male (E) mice. n= 5 per group. Nociceptive
1045 thresholds after SNI and pegDT (pink) or vehicle (white) IT injection in female (F) and
1046 male (G) mice. (H) Nociceptive thresholds at baseline of female WT → WT (black) or
1047 *Penk*$^{-/-}$ → WT (white) bone marrow chimeras. (I) Female *Foxp3*-DTR + *Penk*$^{-/-}$ (1:1) →
1048 WT mice and tested for nociceptive thresholds after pegDT (pink) or vehicle (white) IT,
1049 n=10 per group. (J) Nociceptive thresholds in SNI mice after pegDT (pink) or vehicle
1050 (white) IT injections. (K) WT SNI female mice given low-dose IL-2 and naltrindole. (L)
1051 Nociceptive efficacy calculated as percent compared to baseline threshold. ns = not
1052 significant, *p<0.05, **p<0.01,***p<0.001.
1053
1054
1055
1056

1057 **Figure 5. Treg-derived enkephalin is dispensable for suppressing inflammation.**
1058 (A) Baseline nociceptive thresholds of uninjured *Rag2*$^{+/+,\ +/-\ or\ -/-}$ female mice. (B)
1059 Nociceptive thresholds of female *Foxp3*-DTR mice injected with pegDT IT + IV clodronate
1060 (pink) or control (white) liposomes showing peripheral macrophages do not mediate the
1061 nociception induced by mTreg depletion, n=5 per group. (C) Representative flow
1062 cytometry histograms of proliferated conventional T cells (Tconv) alone (pink) or 4:1 with
1063 WT Tregs (gray), *Penk*$^{-/-}$ Tregs (yellow), or unstimulated, un-proliferated cell trace violet-
1064 stained control (blue). Histogram shows cells that have not proliferated. (D) Suppression
1065 of Tconv cell proliferation by different concentrations of WT Tregs (white) or *Penk*$^{-/-}$ Tregs
1066 (yellow). (E) Schematic representation of competition experiment showing 1:1 transfer of
1067 WT or *Penk*$^{-/-}$ T cells into *Rag2*$^{-/-}$ mice. SNI surgery was performed and organs were
1068 harvested 4 weeks later for F-H. (F) Equal competition of *Penk* sufficient CD45.1 and
1069 *Penk* deficient CD45.2 CD4^{+} T cells in the meninges represented as a concatenated flow
1070 cytometry plot, n=4 per group. Representative flow cytometric plots. (G) Pooled
1071 proportion of *Penk* sufficient CD45.1 and *Penk* deficient CD45.2 CD4^{+} T cells in different
1072 organs, n=4 per genotype. (H) Percent of FoxP3^{+}, IFN-γ^{+} and IL-17A^{+} CD4^{+} T cells from
1073 G. (I) Representative flow cytometric plots of cytokine secretion by CD4^{+} T cells after
1074 GVHD induced by transfer of pre-activated Tconv alone or combined with *Penk*$^{+/+}$ or *Penk*$^{-}$
1075 $^{/-}$ Tregs. (J) Weight curves of GVHD mice, n=3-4 per group. ns = not significant, **p*<0.05,
1076 ***p*<0.01,****p*<0.001. **Related to Figure S5.**
1077
1078 **Figure 6. δOR on MrgprD^{+} sensory neurons is required for mTreg mediated anti-**
1079 **nociception.**
1080 (A) Schematic representation of AAV-induced ablation of *Oprd1* in the PNS (B-C) or CNS.
1081 (B) Nociceptive thresholds of female mice lacking *Oprd1* in the PNS after mTreg
1082 expansion compared to controls. (C) Anti-nociceptive efficacy of mTreg expansion. (D)
1083 No difference in nociceptive thresholds in female mice lacking *Oprd1* in the CNS after
1084 mTreg expansion compared to controls. (E) Heatmap of row normalized expression from
1085 DRG sensory neurons clusters from combined GSE139088 and GSE201653. (F)
1086 Proportions of sensory neuron clusters expressing *Oprd1* from E. (G) Representative flow
1087 cytometry plot of δOR-GFP (green) expression on IB4^{+} MrgprD^{+} DRG sensory neurons
1088 compared to cells from non-reporter mice (purple). Overlaid are lymphoid CD45^{+} CD90.2^{+}
1089 cells and myeloid CD45^{+} CD11b^{+} cells from the DRG. (H-I) Percent response to 0.008 g
1090 von Frey fiber stimulation after SNI in female (H) or male (I) mice conditionally lacking
1091 δOR on MrgprD^{+} neurons (pink) or controls (white). (J) Nociceptive thresholds after
1092 mTreg expansion in female mice lacking *Oprd1* in MrgprD^{+} neurons compared to controls.
1093 (K) Anti-nociceptive efficacy of mTreg expansion. SA-LTMR= Slowly adapting low-
1094 threshold mechanoreceptor, RA-LTMR= rapidly-adapting low-threshold
1095 mechanoreceptor, MrgprD= Mas-related G protein-coupled receptor D, Prop.=
1096 proprioceptor, SST: somatostatin, Trpm8= Transient receptor potential cation channel
1097 subfamily M member 8, TAM= Tamoxifen, cKO= Conditional KO, ns = not significant,
1098 **p*<0.05, ***p*<0.01,****p*<0.001.
1099
1100
1101
1102

Figure 7. mTreg expand during gestation to promote pregnancy induced analgesia (A) Schematic representation of experimental assessment of pregnancy-induced analgesia (PIA) in mice. 4 weeks after SNI, female mice were mated with a syngeneic male. (B) Nociceptive thresholds of pregnant SNI mice before and after delivery, compared to unmated nulliparous mice, n=8-12 per group. (C) Area under the curve (AUC) of nociceptive threshold curves of pregnant mice injected IT with δOR-selective antagonist naltrindole (pink) or vehicle (white). (D) PIA in mice lacking δOR on MrgprD^{+} sensory neurons or controls, n= 4-5 per group. (E) PIA comparing WT or *Rag2*$^{-/-}$ mice, n=13-19. (F) AUC of PIA of *Rag2*$^{-/-}$ mice injected intrathecally with δOR-selective agonist, deltorphin 2, or vehicle during the first 2 trimesters of gestation. (G-J) Representative flow cytometric plots of Tregs and Penk^{+} Tregs in pregnant (pink) compared to nulliparous (white) *Penk*^{Cre}*Rosa26*^{tdTomato} mice with SNI. Mice were harvested on the 12th day of gestation. (K) WT (white) or *Foxp3*-DTR (pink) mice injected with pegDT IT every 4 days demonstrating mTreg dependent PIA. (L) AUC of the PIA as represented in L. ns = not significant, *p<0.05, **p<0.01,***p<0.001. **Related to Figure S6.**

Supplemental Figure Legends

Figure S1. Flow cytometric gating strategy of meningeal Tregs.
(A) Gating strategy to quantify tissue Treg numbers. Numbers indicate gate frequency. Mice were injected IT with ARTC2 nanobody to minimize Treg apoptosis and injected IV with anti-CD45 FITC (pink) antibody or vehicle injected (blue) to label vascular immune cells.

Figure S2. pegDT IT injection avoids systemic inflammation and weight loss in *Foxp3*-DTR mice.
(A) Evan's blue staining after IT injection showing diffusion into the cerebellum, the olfactory bulb, the cervical and lumbar lymph nodes, the spinal cord meninges and the lumbar DRG. (B) pegDyLight650 IT injection exhibits a more limited diffusion than Evan's blue. (C) Weight curves of *Foxp3*-DTR mice injected with IT pegDT, IP DT or IT vehicle every 3 days demonstrating a lack of weight loss after site-selective Treg ablation. Arrows represent DT injections. (D and E) Representative images of spleen sizes and spleen weights from mice in (C). (F) Survival curves of mice in (C). ns = not significant, *$p<0.05$, **$p<0.01$,***$p<0.001$.

Figure S3. mTreg depletion selectively induces mechanical hypersensitivity in female mice.
(A) von Frey, (B) Hargreaves, (C) hotplate, (D) tail flick, (E) acetone, (F) pinprick, (G) brush and (G) rotarod behavioral testing in *FoxP3*-DTR mice injected with a single dose of IT pegDT. n = 4-20 mice per group. ns = not significant,****$p<0.0001$.

Figure S4. mTreg expansion selectively improves mechanical hypersensitivity in injured female mice.
(A) mTreg expansion using IL-2 IT injections induces no changes in nociceptive thresholds in uninjured naive male and female mice. mTreg expansion in nerve-injured mice induces no changes in (B) acetone, (C) Hargreaves and (D) hotplate behavioral testing. ns = not significant.

Figure S5. Functional characterization of enkephalin from CD4$^+$ T cells.
(A) Chimerism of meningeal Tregs and spinal cord microglia in PenkDTR$^{\Delta heme}$ mice and (B) pooled chimerism comparing Tregs in the meninges and in the lymphoid organs compared to tissue macrophages of the spinal cord (microglia) and the epidermis (Langerhans cells, LC). (C) mTreg number after IP DT injection in PenkDTR$^{\Delta heme}$ mice. (D) Weight curves of PenkDTR$^{\Delta heme}$ mice injected with IP DT every three days showing peripheral penk ablation doesn't induce weight loss. (E) Unaltered spleen weight and (F) meningeal and (G) spleen CD4$^+$ T cell populations after IP DT. Unaltered CD4 T cell populations in the (H) spleen and (I) in the nerve and unaltered (J) mouse weight and (K) spleen weight. (L) Graft Versus Host Disease (GVHD) score in *Rag2*$^{-/-}$ mice injected with pre-activated Tconv alone or with *Penk*$^{+/+}$ or *Penk*$^{-/-}$ Tregs, n=3-4 mice per group. (M) IFN-γ$^+$ and (N) IL-17$^+$ CD4$^+$ T cells after GVHD induction. ns = not significant, *$p<0.05$, ***$p<0.001$.

Figure S6. SNI and mTreg depletion does not lead to altered fetal resorption.
(A) Number of resorbed fetuses and (B) number of pups per pregnancy in pregnant sham and SNI mice. (C) Weight of offspring at adulthood from sham and SNI mothers. (D) Number of resorbed fetuses and (E) litter size in WT and *FoxP3*-DTR mothers injected IT with pegDT throughout pregnancy. ns = not significant

References

1. Mogil, J.S. (2012). Sex differences in pain and pain inhibition: multiple explanations of a controversial phenomenon. Nat. Rev. Neurosci. *13*, 859–866. 10.1038/nrn3360.

2. Aloisi, A.M., Bachiocco, V., Costantino, A., Stefani, R., Ceccarelli, I., Bertaccini, A., and Meriggiola, M.C. (2007). Cross-sex hormone administration changes pain in transsexual women and men. Pain *132 Suppl 1*, S60–S67. 10.1016/j.pain.2007.02.006.

3. Petrovski, B.É., Vetvik, K.G., Lundqvist, C., and Eberhard-Gran, M. (2018). Characteristics of menstrual versus non-menstrual migraine during pregnancy: a longitudinal population-based study. J. Headache Pain *19*, 27. 10.1186/s10194-018-0853-3.

4. Negro, A., Delaruelle, Z., Ivanova, T.A., Khan, S., Ornello, R., Raffaelli, B., Terrin, A., Reuter, U., Mitsikostas, D.D., and European Headache Federation School of Advanced Studies (EHF-SAS) (2017). Headache and pregnancy: a systematic review. J. Headache Pain *18*, 106. 10.1186/s10194-017-0816-0.

5. Melhado, E.M., Maciel, J.A., and Guerreiro, C.A.M. (2007). Headache during gestation: evaluation of 1101 women. Can. J. Neurol. Sci. J. Can. Sci. Neurol. *34*, 187–192. 10.1017/s0317167100006028.

6. Gintzler, A.R. (1980). Endorphin-Mediated Increases in Pain Threshold During Pregnancy. Science *210*, 193–195. 10.1126/science.7414330.

7. Ray-Griffith, S.L., Wendel, M.P., Stowe, Z.N., and Magann, E.F. (2018). Chronic pain during pregnancy: a review of the literature. Int. J. Womens Health *10*, 153–164. 10.2147/IJWH.S151845.

8. Burzyn, D., Kuswanto, W., Kolodin, D., Shadrach, J.L., Cerletti, M., Jang, Y., Sefik, E., Tan, T.G., Wagers, A.J., Benoist, C., et al. (2013). A Special Population of Regulatory T Cells Potentiates Muscle Repair. Cell *155*, 1282–1295. 10.1016/j.cell.2013.10.054.

9. Astarita, J.L., Dominguez, C.X., Tan, C., Guillen, J., Pauli, M.L., Labastida, R., Valle, J., Kleinschek, M., Lyons, J., and Zarrin, A.A. (2023). Treg specialization and functions beyond immune suppression. Clin. Exp. Immunol. *211*, 176–183. 10.1093/cei/uxac123.

10. Samstein, R.M., Josefowicz, S.Z., Arvey, A., Treuting, P.M., and Rudensky, A.Y. (2012). Extrathymic generation of regulatory T cells in placental mammals mitigates maternal-fetal conflict. Cell *150*, 29–38. 10.1016/j.cell.2012.05.031.

11. Arpaia, N., Green, J.A., Moltedo, B., Arvey, A., Hemmers, S., Yuan, S., Treuting, P.M., and Rudensky, A.Y. (2015). A Distinct Function of Regulatory T Cells in Tissue Protection. Cell *162*, 1078–1089. 10.1016/j.cell.2015.08.021.

12. Ali, N., Zirak, B., Rodriguez, R.S., Pauli, M.L., Truong, H.-A., Lai, K., Ahn, R., Corbin, K., Lowe, M.M., Scharschmidt, T.C., et al. (2017). Regulatory T Cells in Skin Facilitate Epithelial Stem Cell Differentiation. Cell *169*, 1119-1129.e11. 10.1016/j.cell.2017.05.002.

13. Bapat, S.P., Myoung Suh, J., Fang, S., Liu, S., Zhang, Y., Cheng, A., Zhou, C., Liang, Y., LeBlanc, M., Liddle, C., et al. (2015). Depletion of fat-resident Treg cells prevents age-associated insulin resistance. Nature *528*, 137–141. 10.1038/nature16151.

14. Salvany-Celades, M., Van Der Zwan, A., Benner, M., Setrajcic-Dragos, V., Bougleux Gomes, H.A., Iyer, V., Norwitz, E.R., Strominger, J.L., and Tilburgs, T. (2019). Three Types of Functional Regulatory T Cells Control T Cell Responses at the Human Maternal-Fetal Interface. Cell Rep. *27*, 2537-2547.e5. 10.1016/j.celrep.2019.04.109.

15. Robertson, S.A., Care, A.S., and Moldenhauer, L.M. (2018). Regulatory T cells in embryo implantation and the immune response to pregnancy. J. Clin. Invest. *128*, 4224–4235. 10.1172/JCI122182.

16. Rowe, J.H., Ertelt, J.M., Xin, L., and Way, S.S. (2012). Pregnancy imprints regulatory memory that sustains anergy to fetal antigen. Nature *490*, 102–106. 10.1038/nature11462.

17. Davoli-Ferreira, M., de Lima, K.A., Fonseca, M.M., Guimarães, R.M., Gomes, F.I., Cavallini, M.C., Quadros, A.U., Kusuda, R., Cunha, F.Q., Alves-Filho, J.C., et al. (2020). Regulatory T cells counteract neuropathic pain through inhibition of the Th1 response at the site of peripheral nerve injury. Pain *161*, 1730–1743. 10.1097/j.pain.0000000000001879.

18. Kuhn, J.A., Vainchtein, I.D., Braz, J., Hamel, K., Bernstein, M., Craik, V., Dahlgren, M.W., Ortiz-Carpena, J., Molofsky, A.B., Molofsky, A.V., et al. (2021). Regulatory T-cells inhibit microglia-induced pain hypersensitivity in female mice. eLife *10*, e69056. 10.7554/eLife.69056.

19. Ito, M., Komai, K., Mise-Omata, S., Iizuka-Koga, M., Noguchi, Y., Kondo, T., Sakai, R., Matsuo, K., Nakayama, T., Yoshie, O., et al. (2019). Brain regulatory T cells suppress astrogliosis and potentiate neurological recovery. Nature *565*, 246–250. 10.1038/s41586-018-0824-5.

20. Dombrowski, Y., O'Hagan, T., Dittmer, M., Penalva, R., Mayoral, S.R., Bankhead, P., Fleville, S., Eleftheriadis, G., Zhao, C., Naughton, M., et al. (2017). Regulatory T cells promote myelin regeneration in the central nervous system. Nat. Neurosci. *20*, 674–680. 10.1038/nn.4528.

21. Scherrer, G., Imamachi, N., Cao, Y.-Q., Contet, C., Mennicken, F., O'Donnell, D., Kieffer, B.L., and Basbaum, A.I. (2009). Dissociation of the opioid receptor mechanisms that control mechanical and heat pain. Cell *137*, 1148–1159. 10.1016/j.cell.2009.04.019.

22. François, A., Low, S.A., Sypek, E.I., Christensen, A.J., Sotoudeh, C., Beier, K.T., Ramakrishnan, C., Ritola, K.D., Sharif-Naeini, R., Deisseroth, K., et al. (2017). A Brainstem-Spinal Cord Inhibitory Circuit for Mechanical Pain Modulation by GABA and Enkephalins. Neuron *93*, 822-839.e6. 10.1016/j.neuron.2017.01.008.

23. Wang, D., Tawfik, V.L., Corder, G., Low, S.A., François, A., Basbaum, A.I., and Scherrer, G. (2018). Functional Divergence of Delta and Mu Opioid Receptor Organization in CNS Pain Circuits. Neuron *98*, 90-108.e5. 10.1016/j.neuron.2018.03.002.

24. Sorge, R.E., Mapplebeck, J.C.S., Rosen, S., Beggs, S., Taves, S., Alexander, J.K., Martin, L.J., Austin, J.-S., Sotocinal, S.G., Chen, D., et al. (2015). Different immune cells mediate mechanical pain hypersensitivity in male and female mice. Nat. Neurosci. *18*, 1081–1083. 10.1038/nn.4053.

25. Othy, S., Jairaman, A., Dynes, J.L., Dong, T.X., Tune, C., Yeromin, A.V., Zavala, A., Akunwafo, C., Chen, F., Parker, I., et al. (2020). Regulatory T cells suppress Th17 cell Ca2+ signaling in the spinal cord during murine autoimmune neuroinflammation. Proc. Natl. Acad. Sci. *117*, 20088–20099. 10.1073/pnas.2006895117.

26. Maganin, A.G., Souza, G.R., Fonseca, M.D., Lopes, A.H., Guimarães, R.M., Dagostin, A., Cecilio, N.T., Mendes, A.S., Gonçalves, W.A., Silva, C.E.A., et al. (2022). Meningeal dendritic cells drive neuropathic pain through elevation of the kynurenine metabolic pathway in mice. J. Clin. Invest. *132*. 10.1172/JCI153805.

27. Anderson, K.G., Mayer-Barber, K., Sung, H., Beura, L., James, B.R., Taylor, J.J., Qunaj, L., Griffith, T.S., Vezys, V., Barber, D.L., et al. (2014). Intravascular staining for discrimination of vascular and tissue leukocytes. Nat. Protoc. *9*, 209–222. 10.1038/nprot.2014.005.

28. Pereira, M.M.A., Mahú, I., Seixas, E., Martinéz-Sánchez, N., Kubasova, N., Pirzgalska, R.M., Cohen, P., Dietrich, M.O., López, M., Bernardes, G.J.L., et al. (2017). A brain-sparing diphtheria toxin for chemical genetic ablation of peripheral cell lineages. Nat. Commun. *8*, 14967. 10.1038/ncomms14967.

29. Minarelli, J., Davis, E.L., Dickerson, A., Moore, W.C., Mejia, J.A., Gugala, Z., Olmsted-Davis, E.A., and Davis, A.R. (2019). Characterization of neuromas in peripheral nerves and their effects on heterotopic bone formation. Mol. Pain *15*, 1744806919838191. 10.1177/1744806919838191.

30. Xie, W., Strong, J.A., and Zhang, J.-M. (2017). Active Nerve Regeneration with Failed Target Reinnervation Drives Persistent Neuropathic Pain. eNeuro *4*. 10.1523/ENEURO.0008-17.2017.

31. Graßhoff, H., Comdühr, S., Monne, L.R., Müller, A., Lamprecht, P., Riemekasten, G., and Humrich, J.Y. (2021). Low-Dose IL-2 Therapy in Autoimmune and Rheumatic Diseases. Front. Immunol. *12*, 648408. 10.3389/fimmu.2021.648408.

32. Syrett, C.M., Paneru, B., Sandoval-Heglund, D., Wang, J., Banerjee, S., Sindhava, V., Behrens, E.M., Atchison, M., and Anguera, M.C. (2019). Altered X-chromosome inactivation in T cells may promote sex-biased autoimmune diseases. JCI Insight *4*. 10.1172/jci.insight.126751.

33. Pyfrom, S., Paneru, B., Knox, J.J., Cancro, M.P., Posso, S., Buckner, J.H., and Anguera, M.C. (2021). The dynamic epigenetic regulation of the inactive X chromosome in healthy human B cells is dysregulated in lupus patients. Proc. Natl. Acad. Sci. U. S. A. *118*, e2024624118. 10.1073/pnas.2024624118.

34. Jiwrajka, N., Toothacre, N.E., Beethem, Z.T., Sting, S., Forsyth, K.S., Dubin, A.H., Driscoll, A., Stohl, W., and Anguera, M.C. (2023). Impaired dynamic X-chromosome inactivation maintenance in T cells is a feature of spontaneous murine SLE that is exacerbated in female-biased models. J. Autoimmun. *139*, 103084. 10.1016/j.jaut.2023.103084.

35. Arnold, A.P. (2020). Four Core Genotypes and XY* mouse models: Update on impact on SABV research. Neurosci. Biobehav. Rev. *119*, 1–8. 10.1016/j.neubiorev.2020.09.021.

36. Arnold, A.P., and Chen, X. (2009). What does the "four core genotypes" mouse model tell us about sex differences in the brain and other tissues? Front. Neuroendocrinol. *30*, 1–9. 10.1016/j.yfrne.2008.11.001.

37. Shime, H., Odanaka, M., Tsuiji, M., Matoba, T., Imai, M., Yasumizu, Y., Uraki, R., Minohara, K., Watanabe, M., Bonito, A.J., et al. (2020). Proenkephalin+ regulatory T cells expanded by ultraviolet B exposure maintain skin homeostasis with a healing function. Proc. Natl. Acad. Sci. *117*, 20696–20705. 10.1073/pnas.2000372117.

38. Galván-Peña, S., Leon, J., Chowdhary, K., Michelson, D.A., Vijaykumar, B., Yang, L., Magnuson, A.M., Chen, F., Manickas-Hill, Z., Piechocka-Trocha, A., et al. (2021). Profound Treg perturbations correlate with COVID-19 severity. Proc. Natl. Acad. Sci. *118*, e2111315118. 10.1073/pnas.2111315118.

39. Sjaastad, L.E., Owen, D.L., Joo, S., Knutson, T.P., O'Connor, C.H., McCluskey, B., LaRue, R.S., Langlois, R.A., and Farrar, M.A. (2022). Influenza infection recruits distinct waves of regulatory T cells to the lung that limit lung resident IgA+ B cells. Preprint at bioRxiv, 10.1101/2022.09.19.508325 10.1101/2022.09.19.508325.

40. van der Veeken, J., Glasner, A., Zhong, Y., Hu, W., Wang, Z.-M., Bou-Puerto, R., Charbonnier, L.-M., Chatila, T.A., Leslie, C.S., and Rudensky, A.Y. (2020). The transcription factor Foxp3 shapes regulatory T cell identity by tuning the activity of trans-acting intermediaries. Immunity *53*, 971-984.e5. 10.1016/j.immuni.2020.10.010.

41. Gong, S., Zheng, C., Doughty, M.L., Losos, K., Didkovsky, N., Schambra, U.B., Nowak, N.J., Joyner, A., Leblanc, G., Hatten, M.E., et al. (2003). A gene expression atlas of the central nervous system based on bacterial artificial chromosomes. Nature *425*, 917–925. 10.1038/nature02033.

42. Baysoy, A., Seddu, K., Salloum, T., Dawson, C.A., Lee, J.J., Yang, L., Gal-oz, S., Ner-Gaon, H., Tellier, J., Millan, A., et al. (2023). The interweaved signatures of common-gamma-chain

cytokines across immunologic lineages. J. Exp. Med. *220*, e20222052. 10.1084/jem.20222052.

43. Zamir, N., Palkovits, M., Weber, E., Mezey, E., and Brownstein, M.J. (1984). A dynorphinergic pathway of Leu-enkephalin production in rat substantia nigra. Nature *307*, 643–645. 10.1038/307643a0.

44. Cugurra, A., Mamuladze, T., Rustenhoven, J., Dykstra, T., Beroshvili, G., Greenberg, Z.J., Baker, W., Papadopoulos, Z., Drieu, A., Blackburn, S., et al. (2021). Skull and vertebral bone marrow are myeloid cell reservoirs for the meninges and CNS parenchyma. Science *373*, eabf7844. 10.1126/science.abf7844.

45. Weisser, S.B., van Rooijen, N., and Sly, L.M. (2012). Depletion and Reconstitution of Macrophages in Mice. J. Vis. Exp. JoVE, 4105. 10.3791/4105.

46. Sankaranarayanan, I., Tavares-Ferreira, D., Mwirigi, J.M., Mejia, G.L., Burton, M.D., and Price, T.J. (2023). Inducible co-stimulatory molecule (ICOS) alleviates paclitaxel-induced neuropathic pain via an IL-10-mediated mechanism in female mice. J. Neuroinflammation *20*. 10.1186/s12974-023-02719-8.

47. Laumet, G., Bavencoffe, A., Edralin, J.D., Huo, X.-J., Walters, E.T., Dantzer, R., Heijnen, C.J., and Kavelaars, A. (2020). Interleukin-10 resolves pain hypersensitivity induced by cisplatin by reversing sensory neuron hyperexcitability. PAIN *161*, 2344. 10.1097/j.pain.0000000000001921.

48. Qi, L., Iskols, M., Shi, D., Reddy, P., Walker, C., Lezgiyeva, K., Voisin, T., Pawlak, M., Kuchroo, V.K., Chiu, I.M., et al. (2024). A mouse DRG genetic toolkit reveals morphological and physiological diversity of somatosensory neuron subtypes. Cell *187*, 1508-1526.e16. 10.1016/j.cell.2024.02.006.

49. Rosen, S.F., Ham, B., Drouin, S., Boachie, N., Chabot-Dore, A.-J., Austin, J.-S., Diatchenko, L., and Mogil, J.S. (2017). T-Cell Mediation of Pregnancy Analgesia Affecting Chronic Pain in Mice. J. Neurosci. Off. J. Soc. Neurosci. *37*, 9819–9827. 10.1523/JNEUROSCI.2053-17.2017.

50. Baron, S.A., and Gintzler, A.R. (1984). Pregnancy-induced analgesia: effects of adrenalectomy and glucocorticoid replacement. Brain Res. *321*, 341–346. 10.1016/0006-8993(84)90190-2.

51. Munoz-Suano, A., Kallikourdis, M., Sarris, M., and Betz, A.G. (2012). Regulatory T cells protect from autoimmune arthritis during pregnancy. J. Autoimmun. *38*, J103–J108. 10.1016/j.jaut.2011.09.007.

52. Barry, A.M., Zhao, N., Yang, X., Bennett, D.L., and Baskozos, G. (2023). Deep RNA-seq of male and female murine sensory neuron subtypes after nerve injury. PAIN *164*, 2196. 10.1097/j.pain.0000000000002934.

53. Midavaine, É., Côté, J., Marchand, S., and Sarret, P. (2021). Glial and neuroimmune cell choreography in sexually dimorphic pain signaling. Neurosci. Biobehav. Rev. *125*, 168–192. 10.1016/j.neubiorev.2021.01.023.

54. van Rooijen, D.E., Roelen, D.L., Verduijn, W., Haasnoot, G.W., Huygen, F.J.P.M., Perez, R.S.G.M., Claas, F.H.J., Marinus, J., van Hilten, J.J., and van den Maagdenberg, A.M.J.M. (2012). Genetic HLA Associations in Complex Regional Pain Syndrome With and Without Dystonia. J. Pain *13*, 784–789. 10.1016/j.jpain.2012.05.003.

55. Aubert, N., Purcarea, M., Fornier, M., Cagnet, L., Naturel, M., Casrouge, A., Dietrich, G., Dieu-Nosjean, M.-C., and Marodon, G. (2024). Enkephalin-mediated modulation of basal somatic sensitivity by regulatory T cells in mice. eLife *13*. 10.7554/eLife.91359.1.

56. R, B., Vl, T., D, W., A, F., C, S., Sa, S., P, C., C, B., C, C., K, S., et al. (2014). Delta opioid receptors presynaptically regulate cutaneous mechanosensory neuron input to the spinal cord dorsal horn. Neuron *81*. 10.1016/j.neuron.2014.01.044.

57. G, S., Ta, A., F, S., C, S., G, S.-J., G, G., G, M., and H, S. (1988). Naloxone does not alter the perception of pain induced by electrical and thermal stimulation of the skin in healthy humans. Pain *34*. 10.1016/0304-3959(88)90122-4.

58. A, A., M, H., Al, H., O, H., and A, B. (1999). Estrogen-induced alterations of spinal cord enkephalin gene expression. Pain *83*. 10.1016/s0304-3959(99)00109-8.

59. Adurthi, S., Kumar, M.M., Vinodkumar, H.S., Mukherjee, G., Krishnamurthy, H., Acharya, K.K., Bafna, U.D., Uma, D.K., Abhishekh, B., Krishna, S., et al. (2017). Oestrogen Receptor-α binds the FOXP3 promoter and modulates regulatory T-cell function in human cervical cancer. Sci. Rep. *7*, 17289. 10.1038/s41598-017-17102-w.

60. Nitsche, J.F., Schuller, A.G.P., King, M.A., Zengh, M., Pasternak, G.W., and Pintar, J.E. (2002). Genetic Dissociation of Opiate Tolerance and Physical Dependence in δ-Opioid Receptor-1 and Preproenkephalin Knock-Out Mice. J. Neurosci. *22*, 10906–10913. 10.1523/JNEUROSCI.22-24-10906.2002.

61. Pereira, M.M.A., Mahú, I., Seixas, E., Martinéz-Sánchez, N., Kubasova, N., Pirzgalska, R.M., Cohen, P., Dietrich, M.O., López, M., Bernardes, G.J.L., et al. (2017). A brain-sparing diphtheria toxin for chemical genetic ablation of peripheral cell lineages. Nat. Commun. *8*, 14967. 10.1038/ncomms14967.

62. Sorge, R.E., Martin, L.J., Isbester, K.A., Sotocinal, S.G., Rosen, S., Tuttle, A.H., Wieskopf, J.S., Acland, E.L., Dokova, A., Kadoura, B., et al. (2014). Olfactory exposure to males, including men, causes stress and related analgesia in rodents. Nat. Methods *11*, 629–632. 10.1038/nmeth.2935.

63. Dixon, W.J. (1965). The Up-and-Down Method for Small Samples. J. Am. Stat. Assoc. *60*, 967–978. 10.2307/2283398.

64. Chaplan, S.R., Bach, F.W., Pogrel, J.W., Chung, J.M., and Yaksh, T.L. (1994). Quantitative assessment of tactile allodynia in the rat paw. J. Neurosci. Methods *53*, 55–63. 10.1016/0165-0270(94)90144-9.

65. Shields, S.D., Eckert, W.A., and Basbaum, A.I. (2003). Spared nerve injury model of neuropathic pain in the mouse: a behavioral and anatomic analysis. J. Pain *4*, 465–470. 10.1067/S1526-5900(03)00781-8.

66. Park, Y.-G., Sohn, C.H., Chen, R., McCue, M., Yun, D.H., Drummond, G.T., Ku, T., Evans, N.B., Oak, H.C., Trieu, W., et al. (2018). Protection of tissue physicochemical properties using polyfunctional crosslinkers. Nat. Biotechnol. 10.1038/nbt.4281.

67. Borges da Silva, H., Wang, H., Qian, L.J., Hogquist, K.A., and Jameson, S.C. (2019). ARTC2.2/P2RX7 Signaling during Cell Isolation Distorts Function and Quantification of Tissue-Resident CD8+ T Cell and Invariant NKT Subsets. J. Immunol. *202*, 2153–2163. 10.4049/jimmunol.1801613.

68. Heinen, A.P., Wanke, F., Moos, S., Attig, S., Luche, H., Pal, P.P., Budisa, N., Fehling, H.J., Waisman, A., and Kurschus, F.C. (2014). Improved method to retain cytosolic reporter protein fluorescence while staining for nuclear proteins. Cytom. Part J. Int. Soc. Anal. Cytol. *85*, 621–627. 10.1002/cyto.a.22451.

69. Collison, L.W., and Vignali, D.A.A. (2011). In Vitro Treg Suppression Assays. Methods Mol. Biol. Clifton NJ *707*, 21–37. 10.1007/978-1-61737-979-6_2.

70. Schroeder, M.A., and DiPersio, J.F. (2011). Mouse models of graft-versus-host disease: advances and limitations. Dis. Model. Mech. *4*, 318–333. 10.1242/dmm.006668.

71. Hess, N.J., Hudson, A.W., Hematti, P., and Gumperz, J.E. (2020). Early T Cell Activation Metrics Predict Graft-versus-Host Disease in a Humanized Mouse Model of Hematopoietic Stem Cell Transplantation. J. Immunol. *205*, 272–281. 10.4049/jimmunol.2000054.

72. N, S., K, F., K, L., De, W., Am, K., and Dd, G. (2020). The emergence of transcriptional identity in somatosensory neurons. Nature *577*. 10.1038/s41586-019-1900-1.

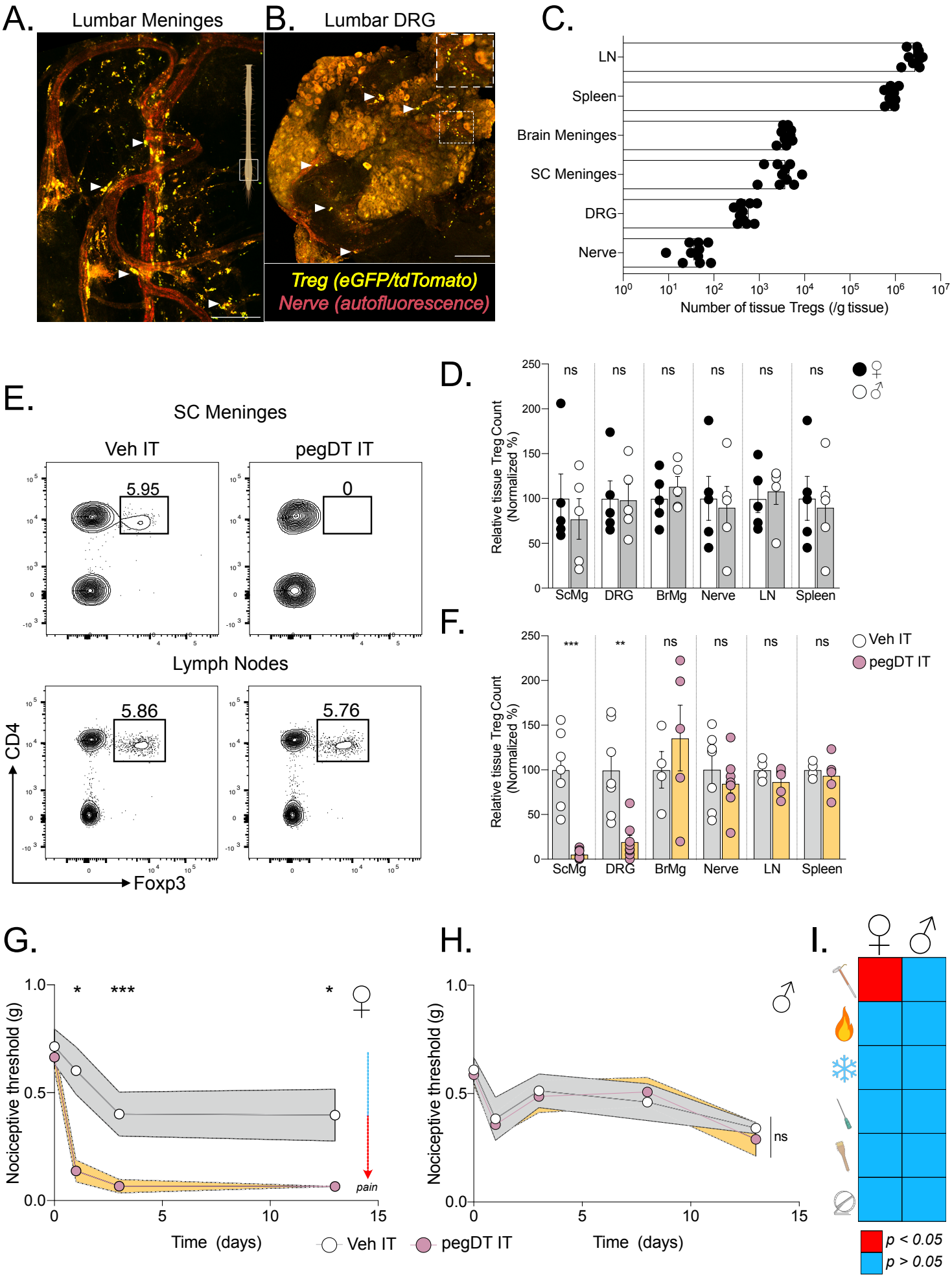
A.
Lumbar Meninges
B.
Lumbar DRG
Treg (eGFP/tdTomato)
Nerve (autofluorescence)
C.
LN
Spleen
Brain Meninges
SC Meninges
DRG
Nerve
Number of tissue Tregs (/g tissue)
D.
Relative tissue Treg Count (Normalized %)
ns
ScMg
DRG
BrMg
Nerve
LN
Spleen
E.
SC Meninges
Veh IT
pegDT IT
5.95
0
Lymph Nodes
5.86
5.76
CD4
Foxp3
F.
Veh IT
pegDT IT
***
**
G.
Nociceptive threshold (g)
Time (days)
pain
H.
I.
p < 0.05
p > 0.05

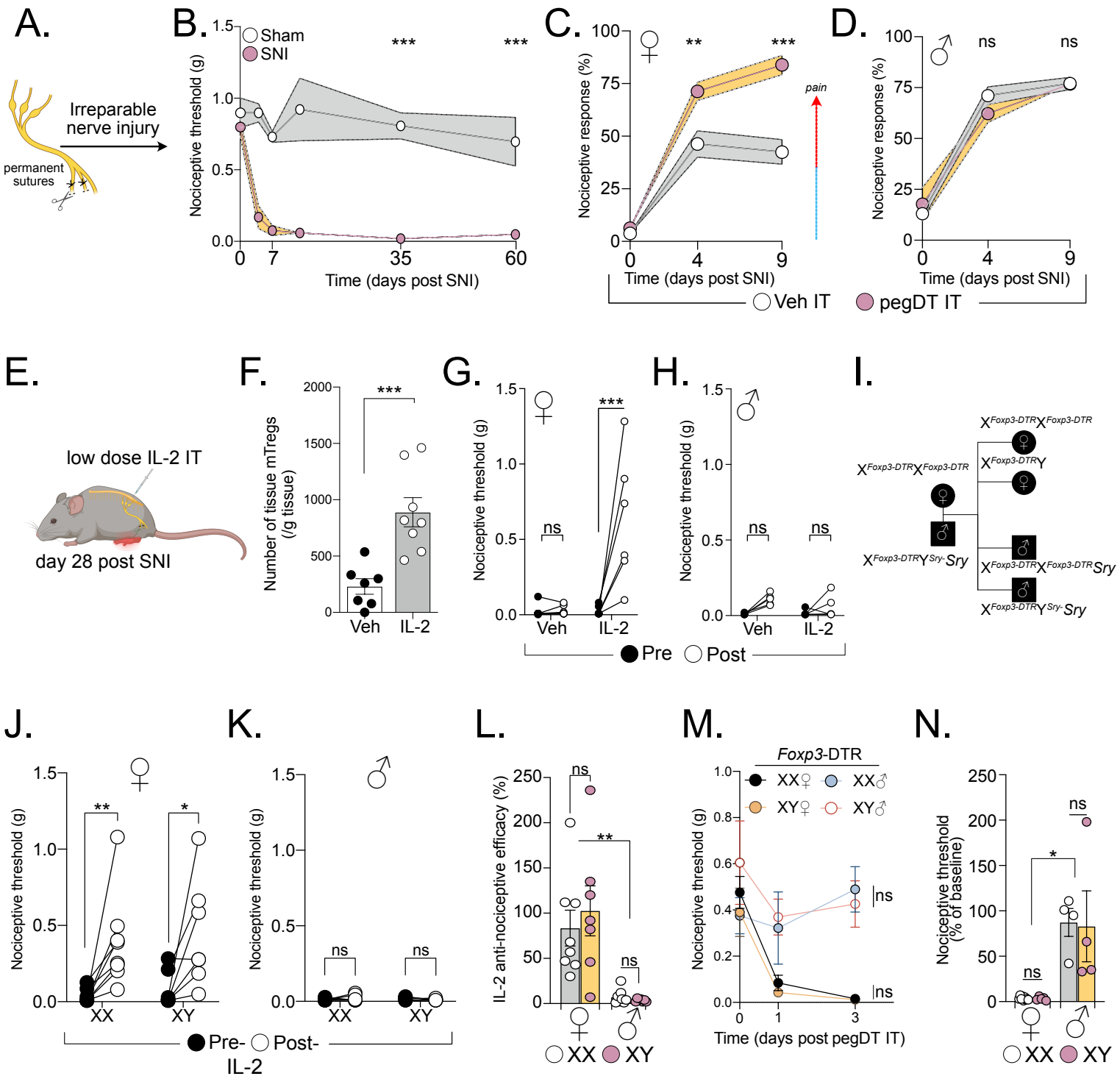
A.
Irreparable nerve injury
permanent sutures
B.
Sham
SNI
Nociceptive threshold (g)
Time (days post SNI)
C.
Nociceptive response (%)
pain
Time (days post SNI)
Veh IT
pegDT IT
D.
Nociceptive response (%)
Time (days post SNI)
E.
low dose IL-2 IT
day 28 post SNI
F.
Number of tissue mTregs (/g tissue)
Veh
IL-2
G.
Nociceptive threshold (g)
Veh
IL-2
H.
Nociceptive threshold (g)
Veh
IL-2
Pre
Post
I.
J.
Nociceptive threshold (g)
XX
XY
K.
Nociceptive threshold (g)
XX
XY
Pre-IL-2
Post-IL-2
L.
IL-2 anti-nociceptive efficacy (%)
XX
XY
M.
Foxp3-DTR
Nociceptive threshold (g)
Time (days post pegDT IT)
N.
Nociceptive threshold (% of baseline)
XX
XY

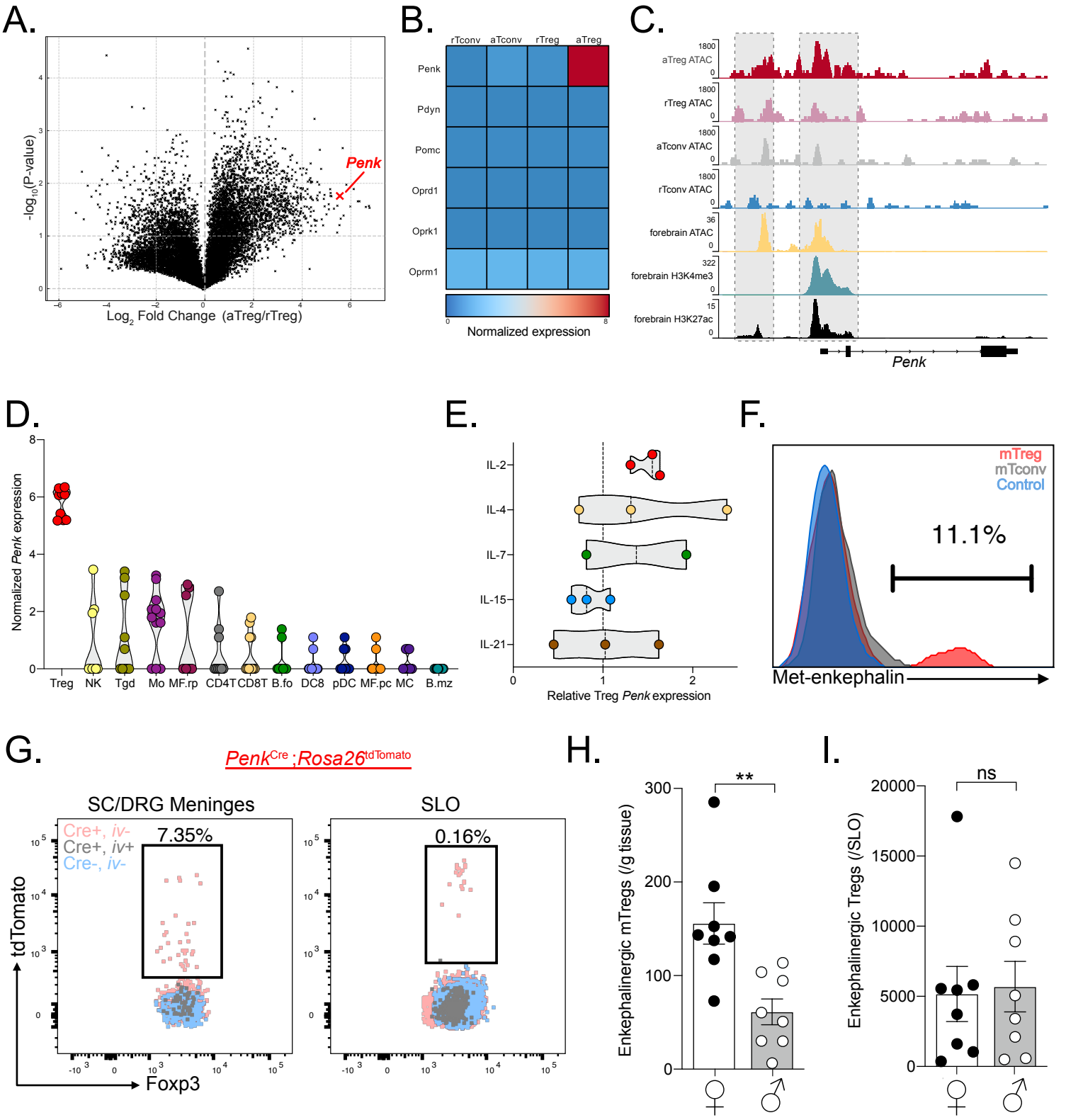
A.
Penk
-log10(P-value)
Log2 Fold Change (aTreg/rTreg)
B.
rTconv aTconv rTreg aTreg
Penk
Pdyn
Pomc
Oprd1
Oprk1
Oprm1
Normalized expression
C.
aTreg ATAC
rTreg ATAC
aTconv ATAC
rTconv ATAC
forebrain ATAC
forebrain H3K4me3
forebrain H3K27ac
Penk
D.
Normalized Penk expression
Treg NK Tgd Mo MF.rp CD4T CD8T B.fo DC8 pDC MF.pc MC B.mz
E.
IL-2
IL-4
IL-7
IL-15
IL-21
Relative Treg Penk expression
F.
mTreg
mTconv
Control
11.1%
Met-enkephalin
G.
PenkCre ;Rosa26tdTomato
SC/DRG Meninges
SLO
Cre+, iv-
Cre+, iv+
Cre-, iv-
7.35%
0.16%
tdTomato
Foxp3
H.
Enkephalinergic mTregs (/g tissue)
**
I.
Enkephalinergic Tregs (/SLO)
ns

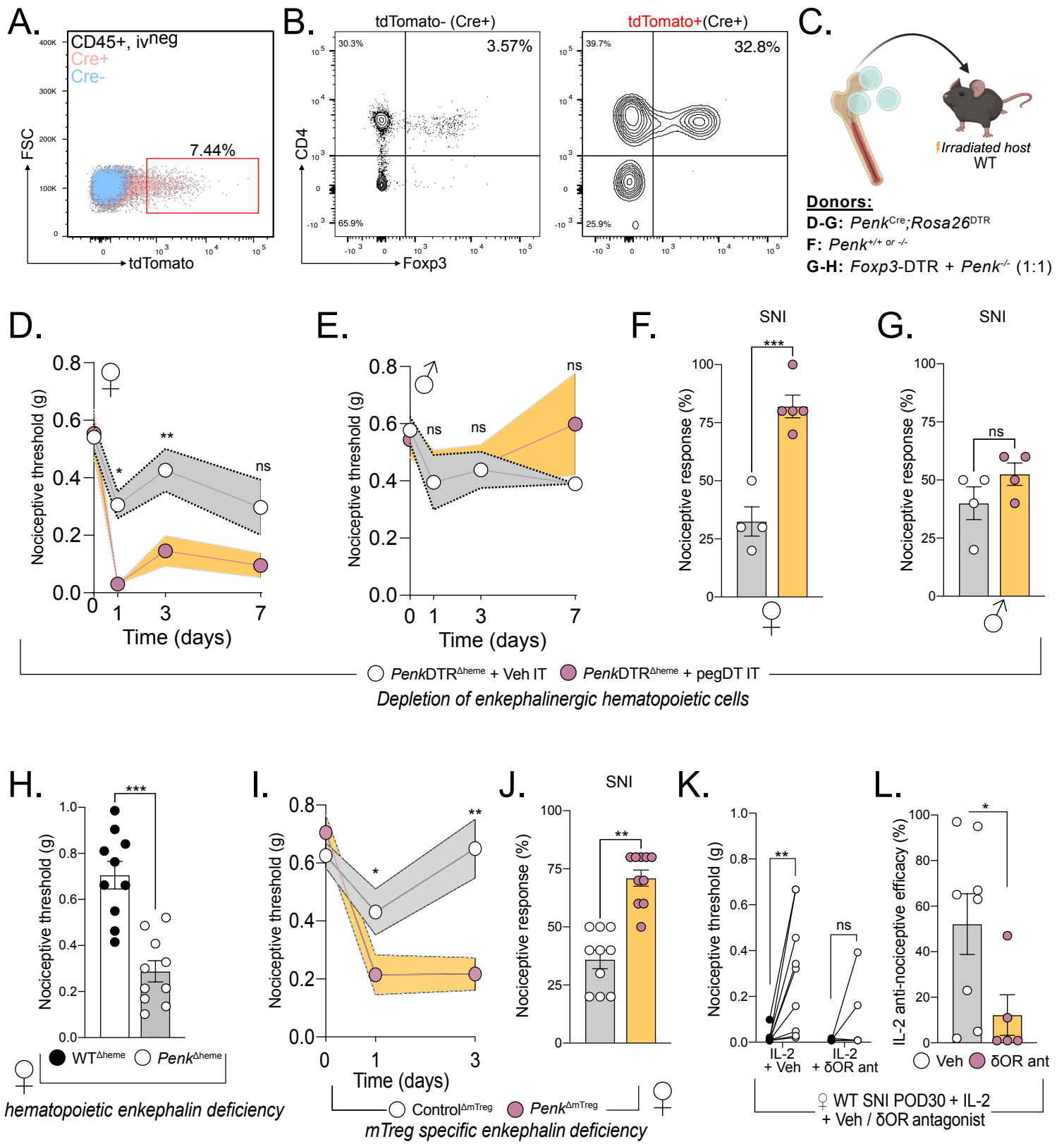
A.
CD45+, ivneg
Cre+
Cre-
7.44%
FSC
tdTomato
B.
tdTomato- (Cre+)
tdTomato+(Cre+)
30.3%
3.57%
65.9%
39.7%
32.8%
25.9%
CD4
Foxp3
C.
Irradiated host
WT
Donors:
D-G: Penk Cre;Rosa26 DTR
F: Penk +/+ or -/-
G-H: Foxp3-DTR + Penk -/- (1:1)
D.
E.
F.
G.
SNI
Nociceptive threshold (g)
Nociceptive response (%)
Time (days)
ns
PenkDTRΔheme + Veh IT
PenkDTRΔheme + pegDT IT
Depletion of enkephalinergic hematopoietic cells
H.
I.
J.
K.
L.
WTΔheme
PenkΔheme
hematopoietic enkephalin deficiency
ControlΔmTreg
PenkΔmTreg
mTreg specific enkephalin deficiency
IL-2 + Veh
IL-2 + δOR ant
IL-2 anti-nociceptive efficacy (%)
Veh
δOR ant
WT SNI POD30 + IL-2 + Veh / δOR antagonist

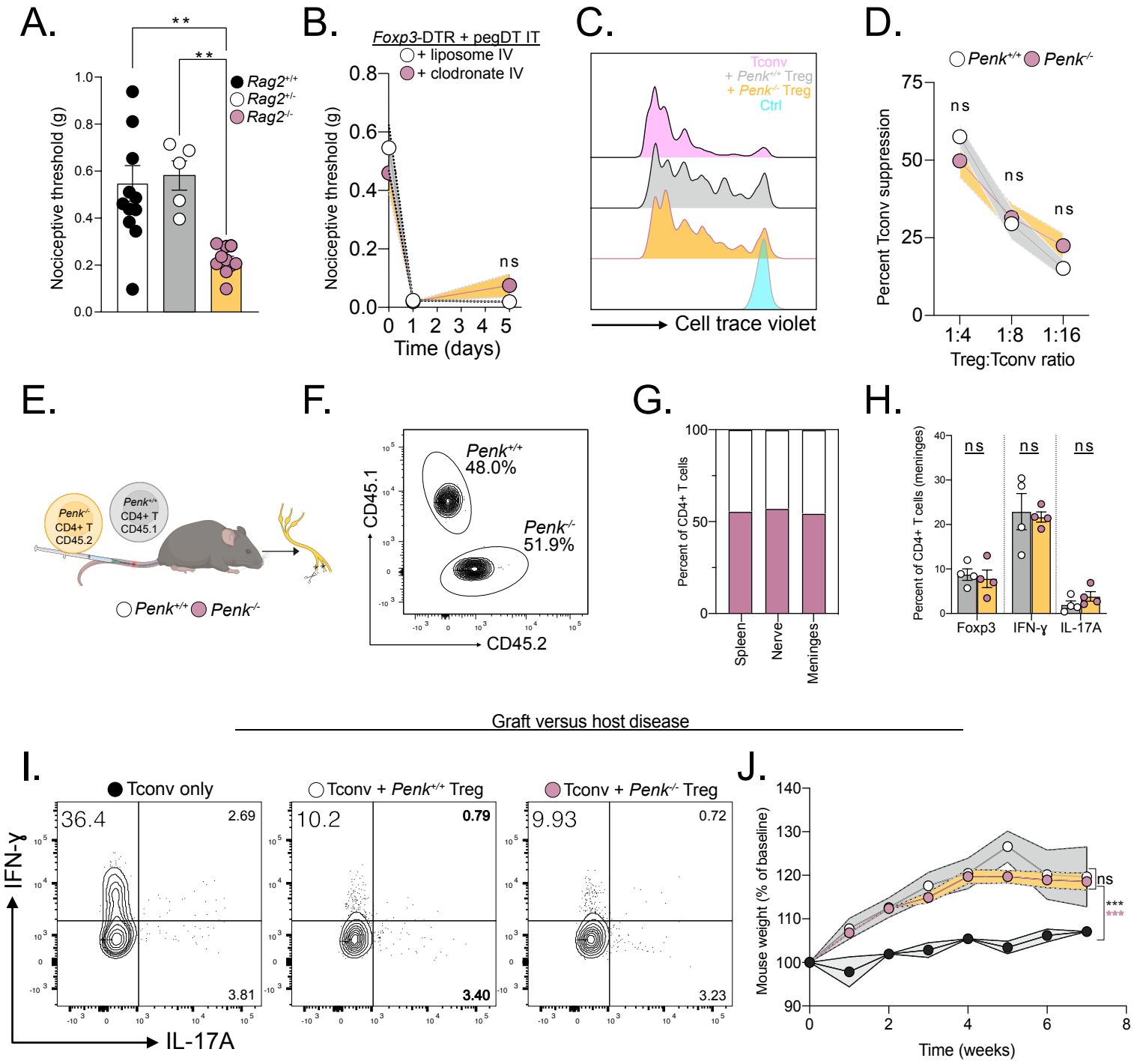
A.
Nociceptive threshold (g)
Rag2+/+
Rag2+/-
Rag2-/-
B.
Foxp3-DTR + pegDT IT
+ liposome IV
+ clodronate IV
Nociceptive threshold (g)
ns
Time (days)
C.
Tconv
+ Penk+/+ Treg
+ Penk-/- Treg
Ctrl
Cell trace violet
D.
Penk+/+ Penk-/-
Percent Tconv suppression
ns
Treg:Tconv ratio
E.
Penk-/- CD4+ T CD45.2
Penk+/+ CD4+ T CD45.1
Penk+/+ Penk-/-
F.
Penk+/+ 48.0%
Penk-/- 51.9%
CD45.1
CD45.2
G.
Percent of CD4+ T cells
Spleen
Nerve
Meninges
H.
Percent of CD4+ T cells (meninges)
ns
Foxp3
IFN-γ
IL-17A
Graft versus host disease
I.
Tconv only
Tconv + Penk+/+ Treg
Tconv + Penk-/- Treg
36.4
2.69
3.81
10.2
0.79
3.40
9.93
0.72
3.23
IFN-γ
IL-17A
J.
Mouse weight (% of baseline)
ns
Time (weeks)

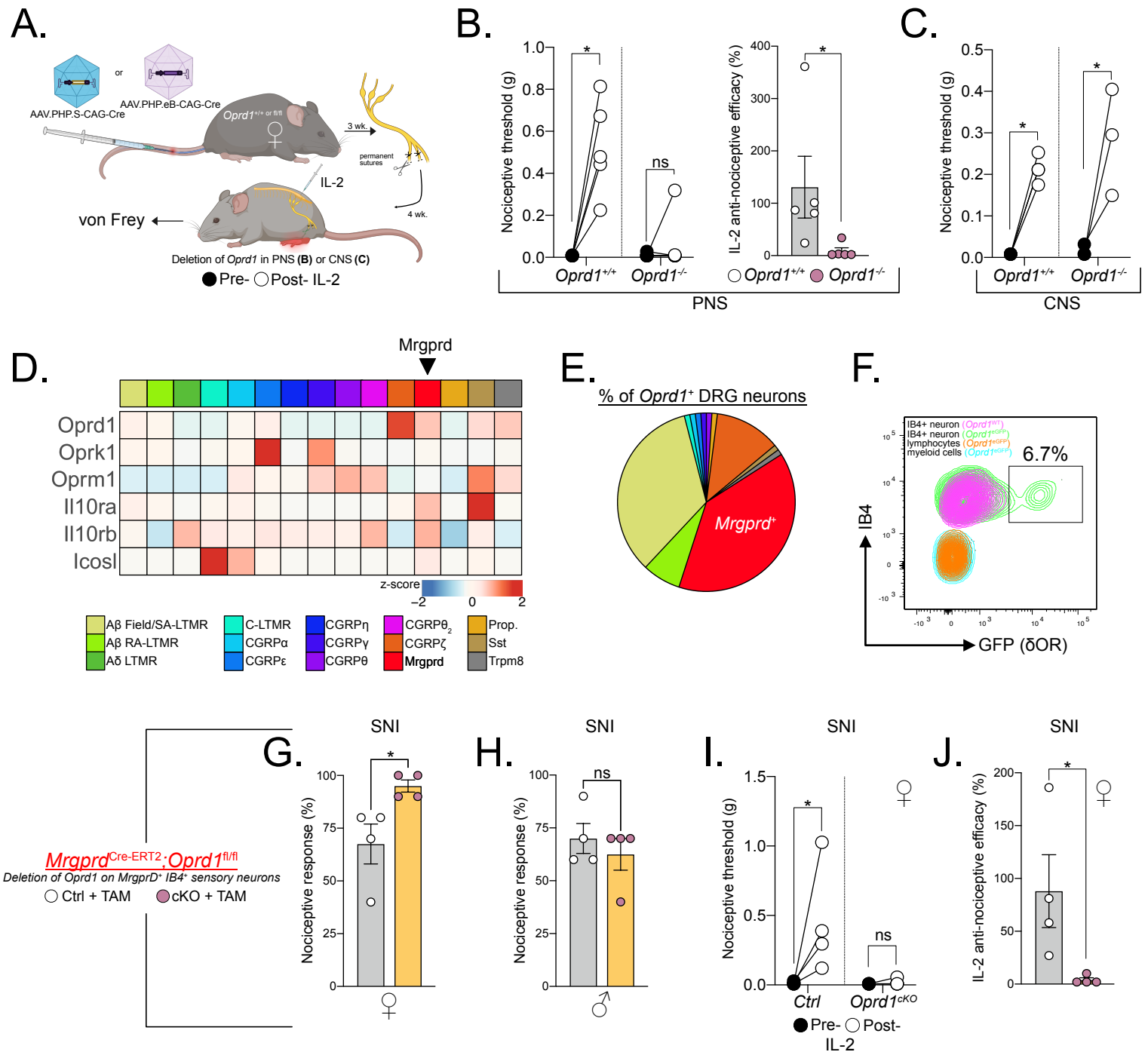
A.
AAV.PHP.S-CAG-Cre
or
AAV.PHP.eB-CAG-Cre
Oprd1+/+ or fl/fl
3 wk.
permanent sutures
IL-2
4 wk.
von Frey
Deletion of Oprd1 in PNS (B) or CNS (C)
Pre- Post- IL-2
B.
Nociceptive threshold (g)
Oprd1+/+
Oprd1-/-
ns
IL-2 anti-nociceptive efficacy (%)
PNS
C.
CNS
D.
Mrgprd
Oprd1
Oprk1
Oprm1
Il10ra
Il10rb
Icosl
z-score
Aβ Field/SA-LTMR
Aβ RA-LTMR
Aδ LTMR
C-LTMR
CGRPα
CGRPε
CGRPη
CGRPγ
CGRPθ
CGRPθ2
CGRPζ
Mrgprd
Prop.
Sst
Trpm8
E.
% of Oprd1+ DRG neurons
Mrgprd+
F.
IB4+ neuron
lymphocytes
myeloid cells
6.7%
IB4
GFP (δOR)
G.
SNI
Mrgprd Cre-ERT2;Oprd1 fl/fl
Deletion of Oprd1 on MrgprD+ IB4+ sensory neurons
Ctrl + TAM
cKO + TAM
Nociceptive response (%)
H.
I.
Nociceptive threshold (g)
Ctrl
Oprd1cKO
J.
IL-2 anti-nociceptive efficacy (%)

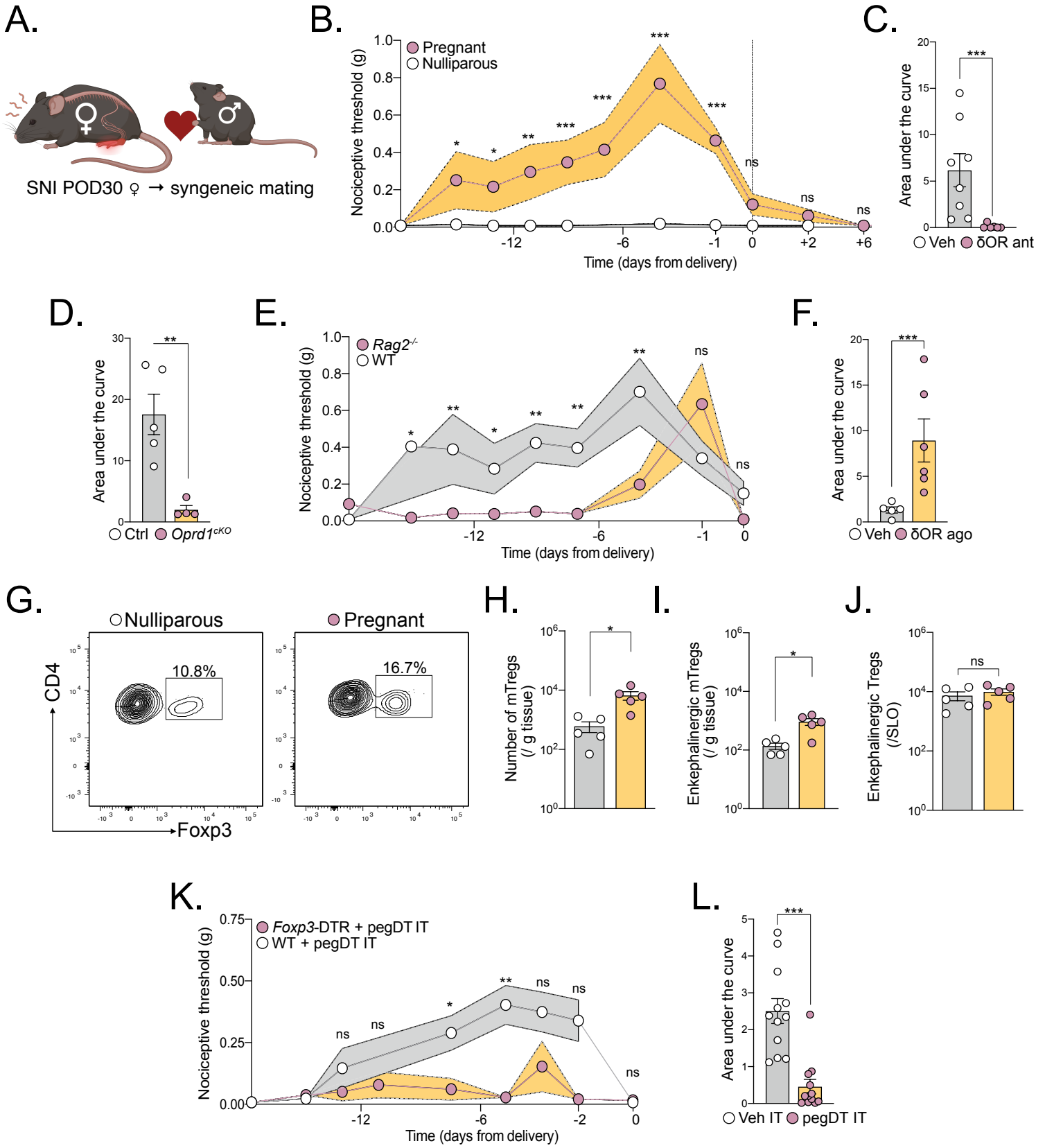
A.
SNI POD30 ♀ → syngeneic mating
B.
Pregnant
Nulliparous
Nociceptive threshold (g)
Time (days from delivery)
C.
Area under the curve
Veh
δOR ant
D.
Area under the curve
Ctrl
Oprd1cKO
E.
Rag2-/-
WT
Nociceptive threshold (g)
Time (days from delivery)
F.
Area under the curve
Veh
δOR ago
G.
Nulliparous
Pregnant
CD4
Foxp3
10.8%
16.7%
H.
Number of mTregs (/ g tissue)
I.
Enkephalinergic mTregs (/ g tissue)
J.
Enkephalinergic Tregs (/SLO)
K.
Foxp3-DTR + pegDT IT
WT + pegDT IT
Nociceptive threshold (g)
Time (days from delivery)
L.
Area under the curve
Veh IT
pegDT IT